DEPARTMENT OF CHEMISTRY, UNIVERSITY OF JYVÄSKYLÄ RESEARCH REPORT No. 170

EXPERIMENTAL AND COMPUTATIONAL STUDIES OF TRANSITION METAL COMPLEXES WITH POLYDENTATE AMINO- AND AMIDOPHENOLATE LIGANDS: SYNTHESIS, STRUCTURE, REACTIVITY AND MAGNETIC PROPERTIES

BY

MIKKO M. HÄNNINEN

Academic Dissertation for the Degree of
Doctor of Philosophy

To be presented, by permission of the Faculty of Mathematics and Science of the University of Jyväskylä, for public examination in Auditorium KEM4, on July 26th, 2013 at 12 noon.

UNIVERSITY OF JYVÄSKYLÄ

Jyväskylä, Finland
ISBN 978-951-39-5302-7
ISSN 0357-346X

ABSTRACT

Hänninen, Mikko M.
Experimental and Computational Studies of Transition Metal Complexes with Polydentate Amino- and Amidophenolate Ligands: Synthesis, Structure, Reactivity and Magnetic Properties
Jyväskylä: University of Jyväskylä, 2013, p. 66
(Department of Chemistry, University of Jyväskylä, Research Report Series
ISSN 0357-346X)
ISBN 978-951-39-5302-7

Chelating polydentate ligands play a key role in several areas of modern coordination chemistry. They can be exploited, for example, in catalysis, bio-inorganic chemistry, heavy metal abstraction and molecular magnetism. Furthermore, compounds of this type can be found in natural chemicals, commercial products and industrial applications. In this dissertation, several 3d, 4d and 5d transition metal complexes with polydentate amino- and amidophenolate ligands were prepared and their structure, reactivity and magnetic properties were studied with experimental and computational techniques.

In the first part of the dissertation, the solid-state structure, reactivity and magnetic properties of 12 novel 3d transition metal complexes were examined. The magnetic behavior of a polynuclear metal complex can be linked to its solid-state structural features to constitute so-called magnetostructural correlations. A clear connection between the M-O-M angles and exchange coupling constants was found in the studied dinuclear Fe(III) complexes. Similar magnetostructural correlations were not equally strong in dinuclear ferromagnetically coupled mixed-valence Mn(II)/Mn(III) system. However, the distortion of the Mn(II) polyhedron from ideal square pyramidal geometry was shown to be related to the strength of the exchange coupling, and together with the M-O-M angle, the nature and strength of the coupling could be estimated.

The second part of this work describes the synthesis and behavior of four novel complexes with heavier 4d and 5d transition metals. Two high-valent molybdenum(VI) complexes with non-innocent tetradentate amidophenolate ligand were prepared and thoroughly characterized using a variety of experimental and computational methods. One of the complexes is the first stable molybdenum(VI) amidophenoxide radical. In addition, the versatility of the bidentate aminophenolate ligands was observed in the synthesis of tungsten(VI) complexes which showed unexpected ligand reactivity upon coordination to a metal cation.

Keywords: amino- and amidophenolate ligands, 3d-5d transition metal complexes, molecular magnetism, single molecule magnets, non-innocent ligands, X-ray crystallography, computational chemistry

Author's address Mikko M. Hänninen
Department of Chemistry
P.O. Box 35
FI-40014 University of Jyväskylä
Finland
mikko.m.hanninen@jyu.fi

Supervisor Professor Reijo Sillanpää
Department of Chemistry
University of Jyväskylä
Jyväskylä, Finland

Co-supervisor Doctor Ari Lehtonen
Department of Chemistry
University of Turku
Turku, Finland

Co-supervisor Doctor Heikki M. Tuononen
Department of Chemistry
University of Jyväskylä
Jyväskylä, Finland

Reviewers Professor Tapani Pakkanen
Department of Chemistry
University of Eastern Finland
Joensuu, Finland

Doctor Christian Lorber
Laboratoire de Chimie de Coordination
University of Toulouse
Toulouse, France

Opponent Professor Peter Edwards
School of Chemistry
Cardiff University
Cardiff, UK

PREFACE

The present research was carried out at the Department of Chemistry, University of Jyväskylä between January 2009 and July 2013.

I wish to express my deepest gratitude to my supervisor Prof. Reijo Sillanpää for the opportunity to join his research group and for his continuous and inspiring guidance throughout this dissertation. I wish to thank Dr. Ari Lehtonen for his important advice and contribution to the experimental part of this work. I am also ever so grateful to Adjunct Prof. Dr. Heikki M. Tuononen for his invaluable guidance in the computational parts of this and several other projects. Furthermore, the contribution from Prof. Enrique Colacio and Prof. Antonio J. Mota to the magnetic studies is deeply appreciated.

I also want to thank all my co-workers in the Department of Chemistry for their advice, instructions and companionship during this project. My colleagues M.Sc Anssi Peuronen and Dr. Jani Moilanen deserve special compliments for withstanding me for all these years. Without our countless discussions many problems would not have been solved (or arisen in the first place).

I'm grateful also to the reviewers of this dissertation, Prof. Tapani Pakkanen and Dr. Christian Lorber, for their valuable comments and suggestions.

This work would not have been finished without the continuous support and help of my beloved family. Furthermore, my dear friends have provided excellent counterbalance to the work, inspiring me and getting me through the harder times during the project.

The financial support from the University of Jyväskylä, Inorganic Materials Chemistry Graduate Program (EMTKO) and Technology Industries of Finland Centennial Foundation is gratefully acknowledged. I'm also very grateful for the CSC – IT Centre for Science for the computing resources they have provided during my work.

Jyväskylä 2.7.2013

Mikko Hänninen

LIST OF ORIGINAL PUBLICATIONS

This dissertation is based on the following original research papers which are herein referred to by their Roman numerals.

I Hänninen, M. M.; Mota, A. J.; Colacio, E.; Sillanpää, R. **A Combined Experimental and Theoretical Study on Bis(μ-alkoxo)diiron(III)Complexes with Hydroxybenzylaminoethanol [O,N,O] Donor Ligands: Syntheses, Structures and Magnetic Properties** *Eur. J. Inorg. Chem.* **2011**, 1990-1996.

II Hänninen, M. M.; Välivaara, J.; Mota, A. J.; Colacio, E.; Lloret, F.; Sillanpää, R. **Ferromagnetic Dinuclear Mixed-Valence Mn(II)/Mn(III) Complexes: Building Blocks for the Higher Nuclearity Complexes. Structure, Magnetic Properties, and Density Functional Theory Calculations** *Inorg. Chem.* **2013**, *52*, 2228-2241.

III Hänninen, M. M.; Sillanpää, R.; Kivelä, H.; Lehtonen, A. **Imidotungsten(VI) Complexes with Chelating Amino and Imino Phenolates** *Dalton Trans.* **2011**, *40*, 2868-2874.

IV Hänninen, M. M.; Paturi, P.; Tuononen, H. M.; Sillanpää, R.; Lehtonen, A. **Heptacoordinated Molybdenum(VI) Complexes of Phenylenediamine Bis(phenolate): A Stable Molybdenum-Amidophenoxide Radical** *Inorg. Chem.* **2013**, *52*, 5714-5721.

Author's contribution

The author of the present study has performed or supervised all the syntheses reported in the original research Papers **I** and **II** and a part of the syntheses in Paper **III**. With regards to computational work, the author of the dissertation has done all the calculations reported in the original research Papers **III** and **IV.** Furthermore, the author has determined all the crystal structures in Papers **I-IV**. The author has written the first manuscript drafts for research Papers **I-IV**.

Other contributions

List of the author's other publications related to the subject but not included in this dissertation.

1. Hänninen, M. M.; Peuronen, A.; Tuononen, H. M. **Do Extremely Bent Allenes Exist?** *Chem. Eur. J.*, **2009**, *15*, 7287-7191.
2. Lauren, E.; Kivelä, H.; Hänninen M.; Lehtonen, A. **Oxidomolybdenum(VI) complexes with atrane-type [O_3N] ligands** *Polyhedron*, **2009**, *28,* 4051-4055
3. Hakala, J.; Hänninen, M. M.; Lehtonen A. **Imidotungsten(VI) complexes with chelating phenols as ROMP catalysts** *Inorg. Chem. Comm.* **2011**, *14,* 1362-1364.
4. Colacio, E.; Perea-Buceta, J. E.; Mota, A. J.; Brechin, E. K.; Prescimone, A.; Hänninen, M.; Seppälä, P.; Sillanpää, R. **Touching the upper limit for ferromagnetic interactions in hetero-bridged dinuclear [Cu_2^{II}] complexes using a novel N_5-dinucleating ligand bearing an endogenous monoatomic amido(R–NH^-)-bridging group** *Chem, Comm.,* **2012**, *48*, 805-807.
5. Riisiö, A.; Hänninen, M. M.; Sillanpää R. **Syntheses and Structural Study of Novel Tetranuclear Bis(phenoxido)-Bridged Cu(II) Metal-organic Macrocycles** *Eur. J. Inorg. Chem.* **2012**, 1048-1053.
6. Peuronen, A.; Hänninen, M. M.; Tuononen, H. M. **Pyrazolium- and 1,2-Cyclopentadiene-based Ligands as σ-Donors: a Theoretical Study of Electronic Structure and Bonding** *Inorg. Chem.* **2012**, *51*, 2577-2587.
7. Farrugia, L. J.; Senn, H. M.; Sillanpää, R.; Hänninen, M. M.; Evans, C. **The QTAIM View of Metal-Metal Bonding in Di- and Trinuclear Disulfido Carbonyl Clusters** *Organometallics* **2012**, *31*, 2559-2570.
8. Palacios, M. A.; Mota. A.J; Ruiz. J.; Hänninen, M. M.; Sillanpää, R.; Colacio, E. **Diphenoxo-Bridged $Ni^{II}Ln^{III}$ Dinuclear Complexes as Platforms for Heterotrimetallic $(Ln^{III}Ni^{II})_2Ru^{III}$ Systems with a High-Magnetic-Moment Ground State: Synthesis, Structure, and Magnetic Properties** *Inorg. Chem.* **2012**, *51*, 7010-7012.
9. Riisiö, A.; Hänninen, M. M.; Sillanpää, R. **Alkyl and diether bridged N,N,N′,N′-tetra(2-hydroxybenzyl)diamines: effects of hydrogen bonding on structure and solubility** *CrystEngComm*, **2012**, *14*, 7258-7263.
10. Colacio, E.; Ruiz. J.; Mota. A.J.; Palacios, M. A.; Ruiz, E.; Cremades, E.; Hänninen, M. M.; Sillanpää, R.; Brechin, E. K. **$Co^{II}Ln^{III}$ dinuclear complexes (Ln^{III} = Gd, Tb, Dy, Ho and Er) as platforms for 1,5-dicyanamide-bridged tetranuclear $Co^{II}_2Ln^{III}_2$ complexes: A magneto-structural and theoretical study** *C. R. Chimie*, **2012**, *15*, 878-888.
11. Riisiö, A.; Lehtonen, A.; Hänninen, M. M.; Sillanpää, R. **Synthesis, Structure and Catalytic Properties of Dinuclear Mo^{VI} Complexes with Ditopic Diaminotetraphenols** *Eur. J. Inorg. Chem.* **2013**, 1499–1508.
12. Sillanpää, R.; Hänninen, M.M. **A cocrystal of two Mo^{VI} complexes bearing different diastereomers of the 2,4-di-tert-butyl-6-{[(1-oxido-1-phenylpropan-2-yl)(methyl)amino]methyl}phenolate ligand derived from (+)-ephedrine** *Acta Cryst.* **2013**, *C69*, 509-512.

CONTENTS

ABBREVIATIONS

acac	Acetylacetonate
dmf	Dimethylformamide
H_2eg	Ethylene glycol
ESR	Electron spin resonance
HOMO	Highest occupied molecular orbital
HPLC	High-performance liquid chromatography
J	Magnetic exchange coupling
NMR	Nuclear magnetic resonance
MOS	Metrical oxidation state
TBP	Trigonal bipyramidal coordination
TLC	Thin layer chromatography
QTM	Quantum tunneling of the magnetization
SMM	Single-molecule magnet
SOMO	Singly occupied molecular orbital
SP	Square pyramidal coordination
T_B	Blocking temperature
U_{eff}	Energy barrier to reversal of the magnetization
χ_M	Molar magnetic susceptibility
ZFS	Zero-field splitting

1 INTRODUCTION

The modern transition metal coordination chemistry is dominated by polydentate ligands exploiting the well-known chelate effect through multiple donor atoms in the molecules. The overall behavior and reactivity of the metal complex is determined by the nature of the metal cation but also by the electronic and steric factors of the coordinated ligands. The polydentate ligands with different types of donors enable the synthesis of diverse molecules from stable, sterically protected mononuclear metal complexes to intricate polynuclear species. These complexes can be utilized in a variety of applications such as catalysis and chemical transformations, medical applications and as biological model compounds. Furthermore, the polynuclear metal complexes are of special importance in the field of molecular magnetism because of the peculiar characteristics of neighboring paramagnetic metal cations.[1]

Single molecule magnets (SMMs) can be described as molecular compounds which show magnetic hysteresis under a certain blocking temperature without any long-range (magnetic) ordering.[2] This relatively new class of compounds possesses vast potential in novel applications such as inventive data storage solutions. In rational design and preparation of the SMMs and other magnetic materials the ligand framework is extremely important. Salen-type ligands (Schiff-bases generally), N-aromatic alcohols and aliphatic polyalcohols have been quite popular in the synthesis of the SMMs, as they are either relatively easy to prepare or they are readily available from commercial sources. A plethora of polynuclear complexes have been prepared and characterized with the above and related ligands, most likely because of the many different coordination modes enabled by multiple donor atoms and the stabilization of the complex by the chelate effect. Rather surprisingly, polydentate aminophenolates are not frequently encountered in the field[2] considering their versatile use in other areas of coordination chemistry.[3,4] However, aminophenols studied in this work form an interesting group of ligands, providing some distinction from traditional Schiff-base ligands with a more flexible backbone and a less dominant nitrogen donor (Figure 1).

In addition to (magnetic) features originating from the metal cations, the reactivity and redox non-innocence of the ligands may induce surprising properties or magnetic behavior for their metal complexes. Commonly, aminophenol-based ligands (excluding the well-known 2-amidophenolates) are thought to be relatively innocent ligands but recently their potential non-innocent behavior has been noticed.[5, 6]

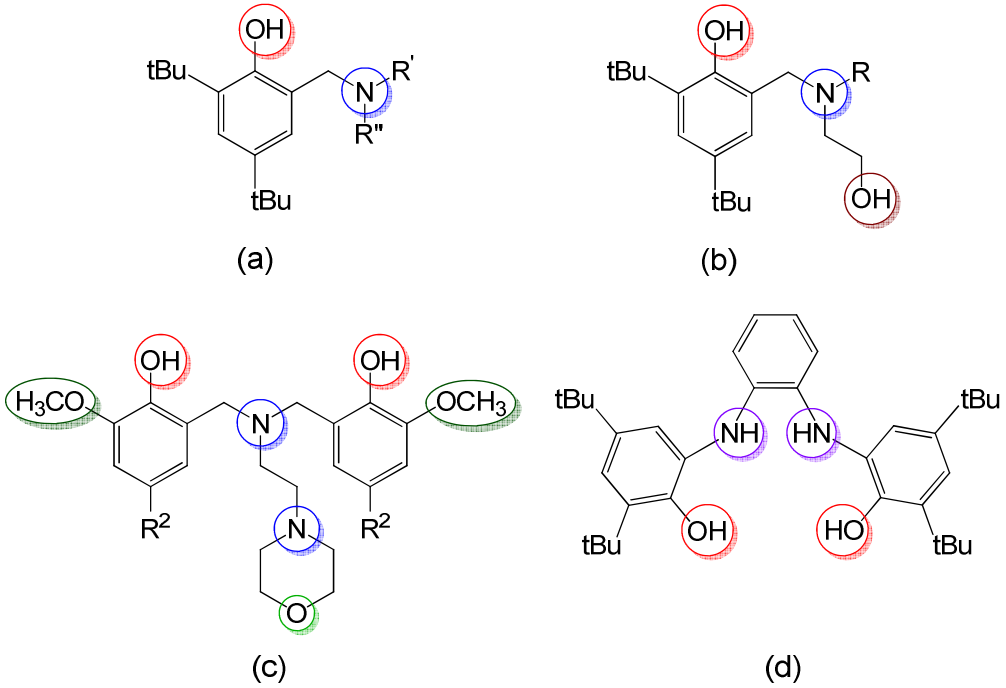

Figure 1. Schematic presentation of polydentate (a) *N*-alkyl- or *N*,*N*-dialkyl-(2-hydroxybenzyl)amine, (b) *N*-ethanol- or *N*-alkyl-*N*-ethanol-(2-hydroxybenzyl)amine, (c) *N*,*N*-bis(2-hydroxybenzyl)amine and (d) *N*,*N*'-bis-(2-hydroxyphenyl)-1,2-phenyldiamine ligand precursors used in this work. The different types of donor groups are highlighted with colored circles.

1.1 Aim of the work

This work was aimed to study the versatility of a relatively simple ligand framework consisting of phenol group(s) with a nitrogen side-arm, and to explore what kind of chemistry can be observed with small changes in these main components. In the first part of the work, relatively simple aminophenolate or aminobisphenolate ligands were exploited to prepare polynuclear 3d transition metal complexes with small structural differences. Crystal structure information obtained by X-ray diffraction is required to be able to interpret the experimentally observed magnetic behavior of the complexes. In some cases, it is also possible to find a correlation between certain structural parameters and magnetic properties (magnetostructural correlations). Furthermore, the complexes prepared with the above ligands should contain reactive sites which can

be utilized in subsequent reactions to synthesize more sophisticated complexes possessing properties such as SMM behavior (see below).

In the second part of the study, potentially reactive or non-innocent amido- and aminophenolate complexes of Mo(VI) and W(VI) cations were studied. The complexes formed were thoroughly investigated by both experimental and theoretical methods to gain further understanding about the electronic distribution and behavior of the ligands and metal ions in the complexes. The substituents at the phenyl ring and at the nitrogen donor atoms have a major influence on the bonding and the coordination capability of the aminophenolates. Moreover, the redox-activity of these ligands can contribute to the electronic properties of the complexes, usually associated only with the metal valence electrons. The comprehension and control of these intrinsic properties can be exploited in the ligand design and in the preparation of new and innovative metal complexes with, for example, interesting reactivity or magnetic features.

2 BACKGROUND OF STUDY

The first section of this chapter aims to introduce the reader to the relatively new concept of molecular nanomagnetism and single-molecule magnets in a rather instructional manner. The basic characteristics of SMMs are introduced and the relevant conditions to obtain the desired behavior are discussed. The second part of the chapter strives to a give compact presentation about the non-innocence or reactivity of ligands and their effects on the compounds itself and on their metal complexes.

2.1 Molecular nanomagnets

Molecular nanomagnetism is a new, rapidly emerging, multidisciplinary research field with exciting applications in the present and future technologies. Although the field is still tempered by a number of practical and fundamental issues, the past few decades of intense research have already produced experimental and theoretical results to direct the future work. The essence of the possible applications is most likely the superior data storage capability hypothesized for hard drives based on molecular nanomagnets compared to drives using traditional magnetic materials.[2,7] Magnetic refrigeration represents another interesting area that could be improved with nanomagnets.[8] In addition to performance enhancements, these molecules can initiate entirely novel branches of industries such as spintronics and quantum computing, because the size of the compounds enables the observation of, and research on, quantum effects such as quantum tunneling.[2,9,10]

Polynuclear transition metal complexes exhibiting superparamagnetic behavior (slow relaxation of the magnetization and magnetic hysteresis) below a certain blocking temperature (T_B) and without 3D magnetic ordering can be defined as single-molecule magnets (SMM); a niche in the world of molecular nanomagnets.[11] The basis of SMM behavior is the existence of an effective energy barrier (U_{eff}, also called anisotropy barrier) preventing the reversal of the

magnetization of the molecule, thus inducing the slow relaxation of magnetization at low temperatures. The height of the energy barrier depends on the high-spin ground state (S_T) and the large *negative* zero-field splitting (D) corresponding to easy-axis magnetic anisotropy, and is given by the equation $S_T^2 \left| D \right|$ or $(S_T^2\text{-}1/4) \left| D \right|$ for integer and half-integer spin ground states, respectively.

The archetype of SMMs, $Mn_{12}Ac$, was structurally characterized already in 1980[12] but its distinctive magnetic properties were not thoroughly investigated until the early 1990s.[2, 13] The metal complex consists of 8 Mn(III) and 4 Mn(IV) cations connected by carboxylate bridges from acetate anions and by triply bridging oxide anions, forming a structure resembling a snow-flake with a distorted octahedral coordination sphere for all manganese cations (Figure 2). The observed magnetic behavior of $Mn_{12}Ac$ indicates that the outer Mn(III) cations (S = 2) are ferromagnetically coupled to each other, while the coupling between the inner Mn(IV) cations (S = 3/2) is antiferromagnetic. The Mn(III)/Mn(IV) interactions are antiferromagnetic, thus producing the desired large-spin ground state (S = 10). Furthermore, the Jahn-Teller axes of the Mn(III) ions are aligned almost parallel leading to a significant negative easy-axis magnetic anisotropy ($D \approx$ -0.5 cm^{-1}).[14] The energy barrier U_{eff} (Figure 2) can be calculated to be 50 cm^{-1} (at 60 K) which held the record for an anisotropy barrier until 2007.[15]

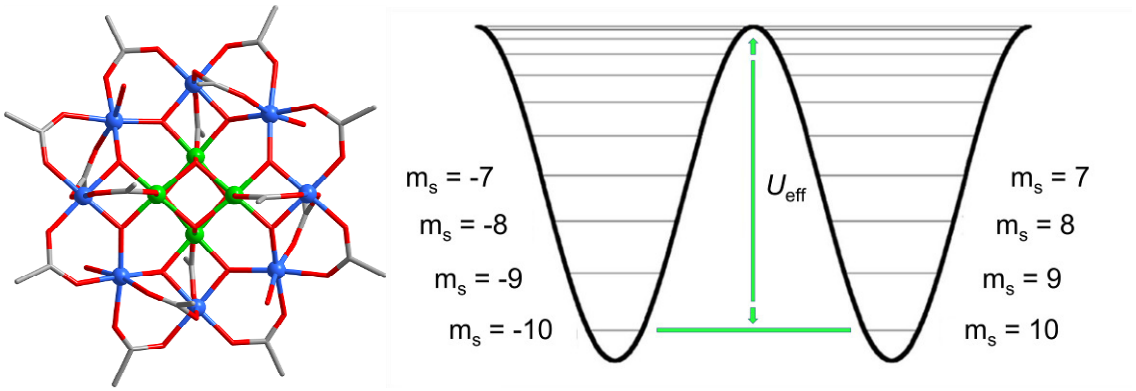

Figure 2. Left: Representation of the structure of $Mn_{12}Ac$. Color code for atoms: *blue*, Mn(III); *green*, Mn(IV); *red*, oxygen; *grey*, carbon. Right: Schematic presentation of the anisotropy barrier (U_{eff}) for the reversal of the magnetization and the non-degenerate (induced by negative zero field splitting) 2S+1 sublevels (m_s) for S = 10 system.

The significant magnetic anisotropy of the $Mn_{12}Ac$ removes the degeneracy of the ground state multiplet, splitting it to 2S+1 sublevels (Figure 2). The m_s = -10 and m_s = +10 states have equal energies, thus making the ground state of the molecule (magnetically) bistable. The height of the energy barrier is related to the thermal relaxation time of the magnetization of the molecule (spin reversal) at specific temperatures. The relaxation slows down considerably at very low temperatures, thus producing a hysteretic behavior of solely molecular origin. In addition to thermal relaxation, quantum tunneling of the magnetization (QTM) through the energy barrier U_{eff} is an effective relaxation route, but also a highly interesting phenomenon with importance in definite applica-

tions.[9a-b, 10c-d] The occurrence of the QTM can be observed as steps in the hysteresis loops in measurements at very low temperatures (Figure 3).[16]

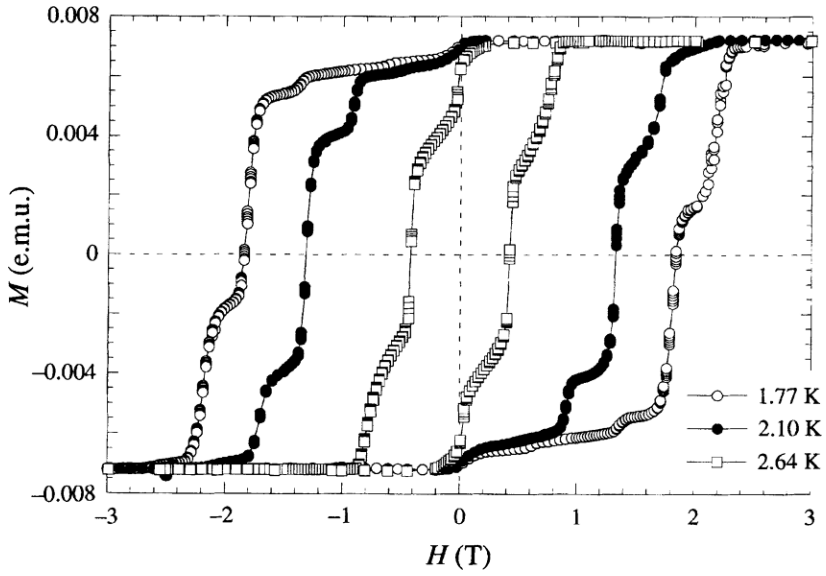

Figure 3. Magnetization hysteresis loops of a single crystal of Mn12Ac at different temperatures, showing the steps originating from the quantum tunneling of magnetization.[16]

What are the origins of the high-spin ground state and large easy-axis magnetic anisotropy and how they can be generated for polynuclear metal complex? A high-spin ground state can be introduced slightly easier since the total spin of the complex is affected by all the paramagnetic centers, and by increasing the number of paramagnetic metal cations, the total spin can be expected to grow *unless* the spins are aligned anti-parallel to each other (*i. e.* having an antiferromagnetic coupling between the metal centers). In this case the total spin of the complex can be 0 or very close to it. On the other hand, if all spins are aligned parallel to each other (*i. e.* ferromagnetic coupling) the S_T is the sum of all individual spins states of the paramagnetic metal cations in the complex and can be quite large, such as an S = 83/2 ground state, which was acquired with a ferromagnetically coupled Mn_{19} aggregate.[17] Hence, the capability to control and predict the interactions between the metal ions would be extremely useful in the rational design of SMMs.

The nature of the coupling between metal ions is essentially determined by exchange interactions between the paramagnetic centers; this includes, for example, direct exchange, superexchange, spin-polarization and double-exchange interactions. In general, all these processes are well-known with a firm theoretical basis and the effects induced by them are relatively predictable in simple systems. However, in the more complicated situations frequently observed in everyday experimental structures, it is not always a straightforward task to recognize which interactions are present and how the observed behavior is formed. For this reason, basic research is needed to be able to design better single-molecule magnets and magnetic materials.

An even more tedious task for an 'SMM engineer' is to mastermind and implement the *easy-axis* magnetic anisotropy to the complexes. Again, the principal theoretical foundations for the phenomena are quite robust but applying them to practical work has proven to be even harder than with the exchange interactions. The different exchange interactions and the origins of magnetic anisotropy are discussed more closely below and some relevant experimental results are presented in Chapter 4.1.2.

Since magnetic bistability is crucial for several applications of the SMMs, chemists have endeavored to raise U_{eff} by synthesizing polynuclear complexes with higher and higher spin ground states and larger magnetic anisotropies. Several synthetic strategies have been used to acquire these properties; most popular one has been the serendipitous synthesis. In this approach, ligands (or ligand precursors) with several coordination modes are mixed with different metal salts and molecular self-assembly is utilized to produce (usually) unpredictable complexes and clusters.[18] The fast progress in the field has provided some theoretical and empirical rules or guidelines which have been applied to develop more sensible routes to obtain complexes showing SMM behavior. More recently introduced rational design principles offer more controllable ways to synthesize complexes with desired properties by using larger (preassembled) ligand frameworks, exploiting concepts of supramolecular chemistry and recognizing the factors generating the high-spin ground state and large magnetic anisotropy for the molecule.[19] Furthermore, a similar strategy can be applied to metal complexes with reactive groups or free coordination sites by subsequent reactions with proper bridging groups and other complexes or metal salts.[20,II]

The theoretical fundamentals for obtaining ferromagnetic exchange interaction and large magnetic anisotropy are relatively complicated and beyond the scope of this work. However, to better understand the experimentally observed magnetic behavior of the prepared complexes, the basic principles of the exchange interactions and their effects on the coupling of paramagnetic metal centers are briefly introduced. In addition, the concept and basis of magnetic anisotropy in metal complexes is discussed at the end of this chapter.

2.1.1 Interactions between magnetic centers

The magnetic interactions in molecular systems are essentially the same that are observed in continuous lattices of magnetic materials, but the importance of the pair interactions (between two metal cations) is pronounced. This is because the molecular systems in general are insulators; thus the magnetic interactions are strongly localized. The coupling between two magnetic centers can be divided into purely magnetic and electrostatic ones corresponding to through-space and through-bond interactions, respectively. However, it can be shown with theoretical calculations that for example between transition metal ions the former interaction is minor compared to the latter. Hence, it can be stated that the basis of the magnetic coupling is the electrostatic interaction which can be compared to the formation of a very weak chemical bond in an extremely simplified ap-

proximation.[2,7] Commonly, the interaction between two paramagnetic centers occurs either directly or through a formally diamagnetic ligand. The former can be generally seen as an exchange interaction while the latter is called superexchange interaction.

Direct and indirect exchange

Direct exchange is present in systems where the metal ions are in close proximity in the way that their (relatively) localized magnetic (singly occupied) orbitals can interact with each other *directly,* generating a strong but short range coupling. The nature of this interaction is dependent on the distance between the nuclei. A short internuclear distance produces antiferromagnetic coupling while a longer separation induces ferromagnetic interactions.[21]

Indirect exchange operates between moments at relatively large distances from each other where there is no direct overlap of the magnetic orbitals. It acts through an intermediary such as 5s and 5p conducting electrons of rare-earth metals. Indirect exchange interaction can be either ferromagnetic or antiferromagnetic.[21] Both of the preceding exchange interactions are mainly operative in pure metals such as iron, cobalt, manganese (direct) or rare-earth metals (indirect) and are thus outside the scope of this study.

Superexchange and spin-polarization

The magnetic interaction of paramagnetic metal ions in *molecules* is generally controlled by superexchange and/or spin-polarization mechanisms. The superexchange mechanism is predominant in metal complexes bridged by single atoms (in contrast to molecular bridges) and is thus of special interest in this work, since in all of the prepared 3d complexes the metal ions are bridged by alkoxide or phenoxide oxygens. The concept of superexchange phenomena was thoroughly studied in the 1950s by Goodenough and Kanamori and a set of semi-empirical rules was developed (known as the Goodenough-Kanamori rules), qualitatively predicting the sign and magnitude of the magnetic exchange coupling in a wide range of materials and molecules.[22]

The interactions between metal cations can be explicated most easily through singly occupied, relatively localized orbitals at the paramagnetic centers (magnetic orbitals). The Goodenough-Kanamori rules state that if these magnetic orbitals are orthogonal to each other, and at the same time have a large overlap density, the spins in the orbitals are aligned parallel, thus producing *ferromagnetic* coupling. On the other hand, if the orbitals have considerable overlap but are non-orthogonal, the spins will preferably orient antiparallel, leading to an *antiferromagnetic* coupling. In the former case the orbitals can be seen as strictly orthogonal (required by the symmetry); this is the case, for example, in the dinuclear copper(II)-oxovanadium(IV) complex in which the magnetic orbitals are $d_{x^2-y^2}$ and d_{xy} for Cu(II) and V(IV), respectively (Figure 4a). The latter situation is present for example in a dinuclear, centrosymmetric Cu(II)-Cu(II) complex where the magnetic orbitals have notable overlap through bridging ligand(s) but because of their non-orthogonality the coupling between these cations has to be antiferromagnetic (Figure 4b). However, the

geometry of the system (for example the M-O-M bridging angles) can force the magnetic orbitals to be "accidentally orthogonal", thus producing ferromagnetic exchange interactions (Figure 4c).[2, 7, 23]

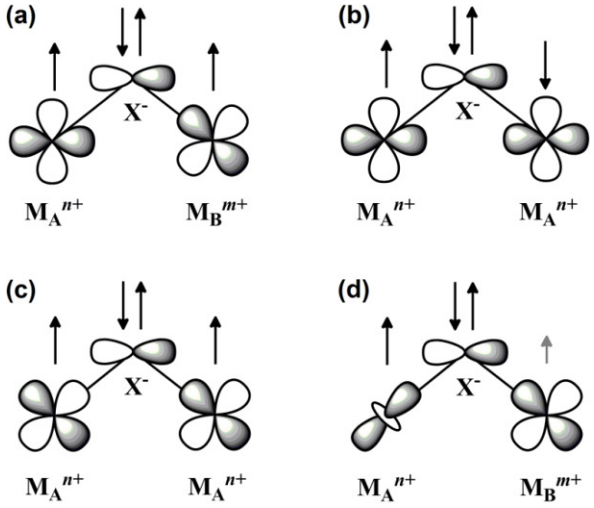

Figure 4. Magnetic orbitals of two transition metal cations connected by a diamagnetic bridging atom (ion) showing strictly orthogonal (a), non-orthogonal (b) accidentally orthogonal orbitals (c) and singly occupied and empty orbital for the spin-polarization mechanism (d).

The spin-polarization mechanism is responsible for the ferromagnetic interactions through overlap between the magnetic orbital of one ion with the empty orbital of another ion. This is the case when, for example, the magnetic d_{z^2} orbital of Mn(III) has non-zero overlap with the empty $d_{x^2-y^2}$ orbital of a neighboring metal cation (Figure 4d). This can be explicated in the way that a fraction of the unpaired electrons from the d_{z^2} orbital is transferred to the empty $d_{x^2-y^2}$ orbital and this, according to Hund's rule, will polarize the unpaired electron density in the d_{z^2} orbital.[2, 7]

Double exchange (spin-dependent delocalization)

For mixed-valence systems (for example, metal complexes with cations in different oxidation states) an additional type of magnetic interaction is encountered. In these compounds the valences may be trapped or partially or completely delocalized (Class I, II or III according to Robin and Day classification).[24] Class I corresponds to the complexes where the well-defined charges can be clearly assigned to each metal, while in Class III compounds the charge is completely delocalized as one or more electrons can rapidly leap from one center to another (Figure 5). The Class II complexes can be seen as an intermediate species between Classes I and III. The magnetic behavior of complexes falling to Class I can be described by the preceding exchange mechanisms, but in case of Class II and III compounds additional contributions from the delocalization of the unpaired electron(s) have to be taken into account. As presented in Figure 5, it is apparent that the leaping electron from Mn(II) must retain its spin parallel

to the Mn(III) electrons (according to the Pauli principle); hence, the double exchange mechanism induces a ferromagnetic coupling between the two magnetic centers.[2]

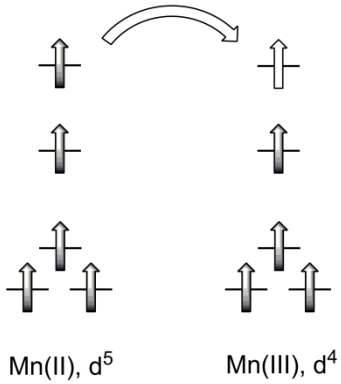

Figure 5. Schematic presentation of the electron configuration of Mn(II) and Mn(III) cations and the partial electron transfer process responsible for double exchange phenomena.

2.1.2 Magnetic anisotropy

Magnetic anisotropy can be described as the directional dependence of magnetic properties of the material. In the absence of an applied magnetic field, the magnetic moment of an anisotropic material is aligned towards one of the easy axes, defined as an energetically favorable direction of spontaneous magnetization. Magnetic anisotropy is of special interest in the design of SMMs. The increase of the anisotropy seems to be a more effective strategy for increasing the anisotropy barrier U_{eff} and blocking temperature T_B than the ever-larger total spins of the compounds, as have been recently demonstrated with several lanthanide-based SMMs (Ln-SMMs).[25,26,27] In general, the axial zero-field splitting (D) is responsible for the magnetic anisotropy in metal complexes. The ZFS phenomena can be defined as the removal of the degeneracy of the spin microstates by a molecular electronic structure (spin-orbit coupling) and/or spin density distribution *in the absence of an external magnetic field*. Since ZFS is usually large in lanthanide cations (which also generally possess large intrinsic spin ground states), they are a good choice in the design of novel SMMs.

The magnetic anisotropy at the molecular level is a sum of several factors, such as the single-ion anisotropy of the metal ions, the anisotropic exchange interactions between the ions and magnetic dipolar interactions (often dominated by the single-ion anisotropy). Molecular architecture plays a key role when determining how the molecular magnetic anisotropy arises from the single-ion anisotropy. Negative molecular D values (D_{mol}) can be obtained, for example, by a collinear alignment of the easy axes of the anisotropic metal ions in the molecule. In general, the two opposite directions of the easy axis are equivalent and the direction of magnetization can be along either one of them. A simple schematic presentation of the arrangement of the single-ion easy axes to obtain negative D_{mol} values is presented in Figure 6.[28]

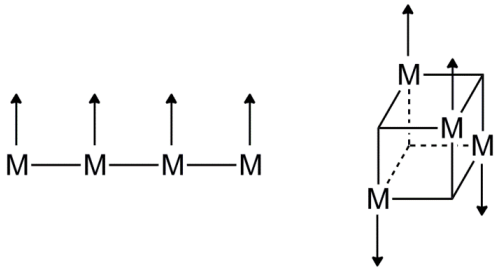

Figure 6. Examples of the collinear easy-axis alignments essential for negative D_{mol} values. Arrows represent the single ion easy axes.

Ligand effects on the magnetic anisotropy

Recent studies have demonstrated that the ligand framework can have a major impact on the magnetic anisotropy and thus on the overall magnetic properties of metal complexes. For example, it has been shown that the π-donor and π-acceptor ligands in the axial position of octahedral Cr(III) complexes have diverse effects on the anisotropy of the metal cation. The π-acceptor ligands cause the magnetic anisotropy to be of the easy-axis type ($D < 0$), while π-donor ligands were found to produce easy plane type magnetic anisotropy ($D > 0$).[29] Furthermore, peripheral ligands can also have a considerable influence on the magnetic behavior of transition metal complexes. Changes in the ligand substituents of the mononuclear square pyramidal Co(II) complex modulated the coordination environment of the metal center, thus enhancing the slow relaxation of magnetization induced by the significant spin-orbit coupling.[30] The possibilities to control and direct the SMM behavior of metal complexes with ligands were also pointed out in a study of the electronic structure of f-elements. A simple model can predict the shape of the 4f electron density of certain lanthanide trications (oblate or prolate), which in turn can be exploited when designing the ligand framework to provide a suitable crystal field to maximize the single-ion anisotropy.[25] Although the magnetic properties of molecules are generally thought to originate from the paramagnetic metal centers, the surrounding ligands are of special importance in the rational design of SMMs and other magnetic materials.

2.2 Non-innocence and reactivity of ligands

2.2.1 Non-innocence of ligands

The behavior of a metal complex is a combination of the intrinsic properties of the metal cation and the features of the coordinating ligands. The ligand affects the reactivity of the metal cation, and thus the whole complex, by steric and electronic factors via the donor atoms. In general, the reactivity is one of the most important attributes of the metal complex as its performance in virtually any given application is closely related to its reactivity. Depending on the stud-

ied system, the complex is desired to be either labile, inert or, as in most occasions, somewhere between these two extremes.

In traditional coordination chemistry, ligands have been thought to be "innocent" *i.e.*, they do not contribute to the redox processes taking place in the complex. This is certainly not true. The "non-innocence" of ligands has always been around, but especially in the description of chemical reactivity it has only recently become a frequently distinguished property.[31] Originally the non-innocence was conversely described by Jørgensen as follows: "Ligands are innocent when they allow oxidation states of the central atoms to be defined".[32] Hence, the redox non-innocent ligands can be depicted as redox-active ligands that can be easily oxidized or reduced without the oxidation or reduction of the metal ion. Commonly these compounds transform into ligand radicals when coordinating to a metal cation, leading to ambiguous electronic structures.

It is important to notice that ligands classified as non-innocent may not behave as non-innocent in all complexes and *vice versa*. Hence, the non-innocence of the ligand has to be described more as a behavioral property than a constant one.[33] Examples of ligands that have been reported to exhibit non-innocent behavior are numerous: α-diimines (a), dialkylglyoximes (b), *o*-quinonediimines (c), *o*-quinones (d) and polycyano compounds (e), to name a few (Figure 7). These and many more ligands are introduced and their redox chemistry thoroughly discussed in a recent article by Kaim.[33a]

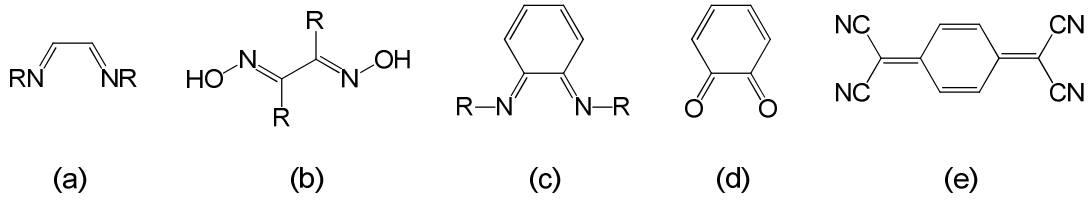

Figure 7. Schematic presentation of some ligands with reported non-innocent behavior (a-e).

The non-innocence of a ligand can be determined and studied with spectroscopic and electrochemical methods such as ESR, UV-VIS spectroscopy and cyclic voltammetry or by a combination of these (spectroelectrochemistry). However, the changes in the oxidation state of the ligand are generally visible also in the geometrical parameters of the solid-state structures of their complexes. With certain non-innocent ligands the effects of the ligand oxidation state can be easily seen from a simple Lewis structure (for example from the amidophenoxide complexes, Figure 8). The changes in the specific C-C, C-N and C-O bond lengths have been known for a while and they can qualitatively be used to assign the oxidation state of the ligand.[34] In addition, based on the analysis of the reported structures with unambiguous oxidation states, the relevant bond distances were related to a single parameter (metrical oxidation state, MOS) that empirically represents the expected ligand oxidation state.[35] Modern computational chemistry and especially DFT methods are also valuable tools in the study of the electronic distribution in the non-innocent ligands and their metal complexes.[36,37]

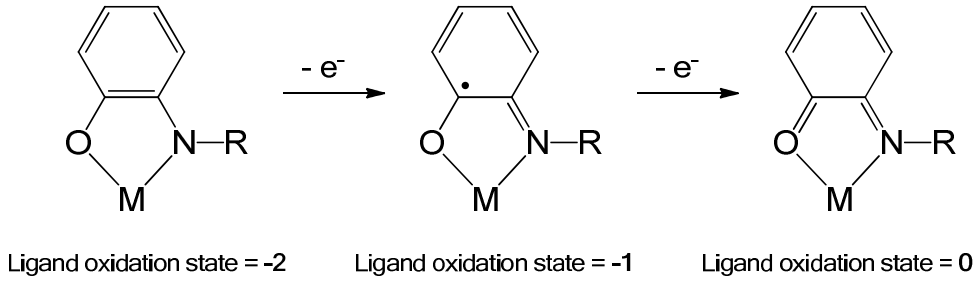

Figure 8. Lewis structures of the possible oxidation states of an amidophenolate ligand.

Non-innocent ligands have been successfully used together with metal ions to achieve significant chemical and physical properties. Typical applications include, for example, molecular magnets/conductors and spin carriers or superexchange mediators.[38,39] Furthermore, these ligands have opened pathways for important synthetic conversion using base metals instead of their noble congeners.[40]

2.2.2 Reactivity of ligands

Non-innocence of the ligands is typically associated with their redox-activity when bound to a metal cation. However, the coordination of a ligand to a metal center alters its characteristics and properties, thus affecting the reactivity of the ligand and possibly enabling reactions which would not take place without the coordination. The ligands that take part in bond activation reactions and/or undergo chemical transformations upon coordination could also be classified as non-innocent. In principle, this behavior provides the basis for metal-catalyzed reactions but it can also be used, for example, in stoichiometric organic synthesis of novel products after the elimination of the product from the coordination sphere.

The determination of the reactive sites in coordinated ligands and the prediction of ligand reactivity is by no means an easy task; thus computational chemistry is frequently utilized to identify these centers and further explicate the observed reactivity. In general, the pathways for these reactions can be considered through a HOMO-LUMO gap of the reactants. When the gap is small, the most plausible pathway for the reactions would be the $HOMO_{donor}$-$LUMO_{acceptor}$ interaction, as the reaction is usually expected to take place between two centers with the greatest difference in the electron density in frontier molecular orbitals. When the HOMO-LUMO gap is large, the electrostatic components are responsible for the interaction between the atomic centers. However, a simple electrostatic inspection of the reactants can be used in several occasions to qualitatively determine the reaction centers of the interacting molecules.[41]

Multiple factors affect to the reactivity of ligands. In general, the electron donor/acceptor properties of the ligand and the metal center are most important while the co-ligands may also play a role. A metal ion's position in the periodic table, its oxidation state and coordination number are the most com-

mon features that govern the behavior of metal and thus mostly affect its coordinating ligands. In addition, the electronic properties of the ligands have a prominent effect on the redox potential of whole complex which in turn has an influence to the overall reactivity of the compound. Furthermore, co-ligands with an electron donor/acceptor ability can assist the metal cation to activate the actual ligand. For example, a strong electron donor can promote the activation of an overall weaker electron donor towards electrophilic attack. The well-known *trans*-effect is also a good example of the role of co-ligands in general ligand reactivity.[41]

Nucleophilic or electrophilic addition to ligands is the most common reaction promoted by their coordination to metal centers. Other types of reactivity, such as acid-base and related reactions, template synthesis and metal-induced rearrangements can also be perceived (Figure 9).[42]

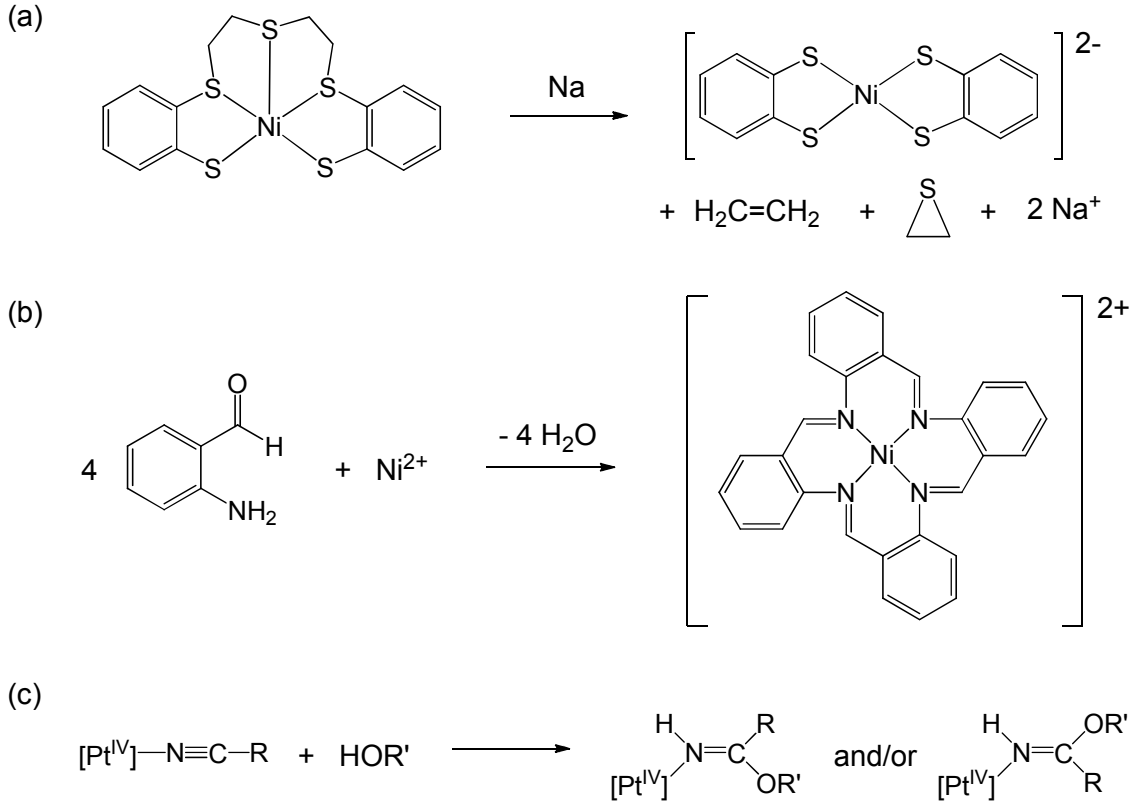

Figure 9. Examples of (a) acid-base (or related) reactions, (b) template synthesis and (c) metal-induced rearrangement reactions of coordinated ligands.

The ligand coupling or redox reactions without any external components (oxidizing or reducing agents, halogenating or alkylating compounds etc.) are of special interest in this dissertation, since this type of ligand reactivity has been previously observed for ligands (or similar to the ones) studied in this work (Figure 10).[6, 43]

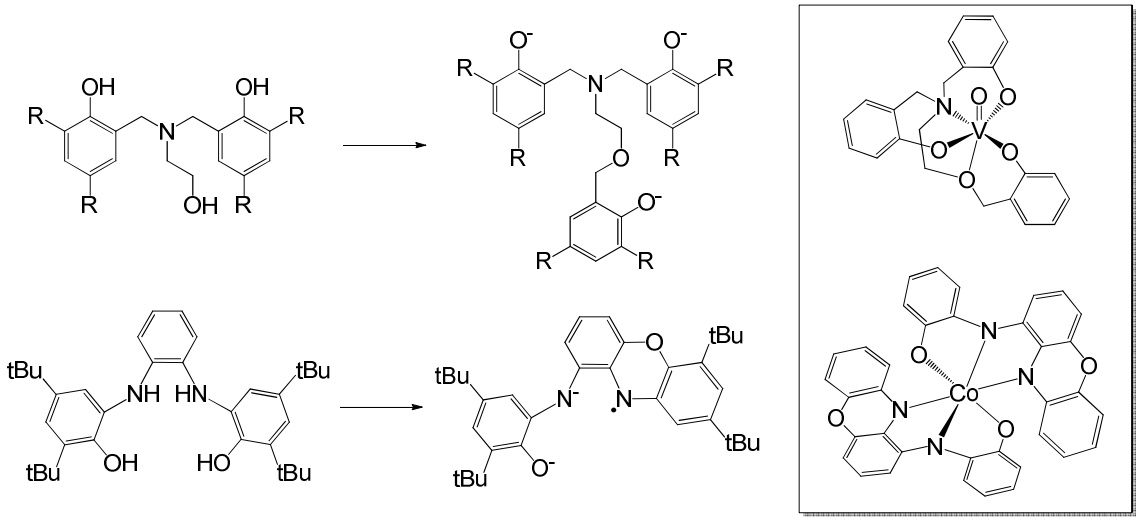

Figure 10. Examples of ligand precursor reactivity upon metal coordination. In the schemes of the complexes the substituents of the phenol rings are omitted for clarity.[6,43]

Several examples of ligand transformation can be found in the literature. When the transformations are reversible, the ligands can be entitled "cooperative", as they function in synergy with the metal cation thus facilitating the chemical reaction.[44] If the transformation is irreversible, the possibility for a catalytic cycle is lost and thus only stoichiometric reactions are feasible. However, with this type of ligand alteration, completely novel reactivity such as C-N bond cleavage, P-Cl bond formation and hydride abstraction, can be discovered.[6,45,46,47] When the redox-activity and structurally non-innocent features of the ligand are combined, even more remarkable reactivity can be observed. Examples of this are the reversible C-C bond formation or generation of a new (also redox-active) ligand with considerably different geometry compared to the original ligand.[43,48] The driving force in many of these ligand-coupling reactions is most likely the high stability of the five- or six-membered chelates that can be formed with the coupled ligand and the metal center (Figure 10).

As shown in the above paragraphs, redox-activity and unexpected reactivity of the ligands can result in metal complexes with either extremely interesting properties and behavior, or previously unknown variants of the ligands which might be difficult to synthesize using traditional (organic) synthetic procedures. Hence the non-innocence of the ligands can play a significant role in various areas of modern coordination chemistry, including molecular magnetism and SMMs, catalysis, bio-inorganic chemistry and general synthesis of the novel ligands and complexes.

3 EXPERIMENTAL

3.1 Ligand synthesis

Polydentate aminophenol and aminobisphenol ligand precursors H_2**L1-L4** were synthesized using recently developed solvent-free thermal oven condensation reactions.[49] This method has numerous advantages over traditional heating or refluxing, in which the yields are low and the reaction times are considerably longer. A schematic presentation of the ligand preparation is presented in Figure 11; the general experimental procedures are described below.

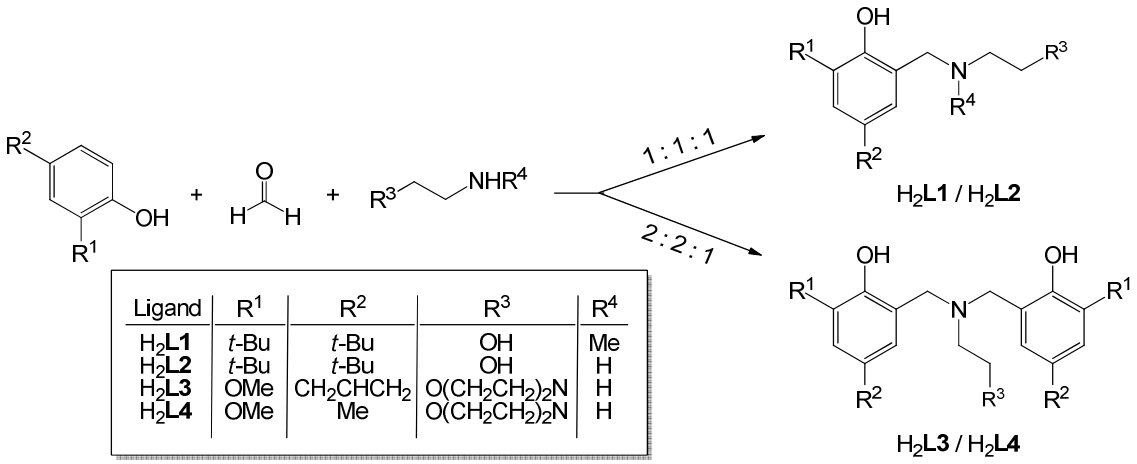

Ligand	R^1	R^2	R^3	R^4
H_2**L1**	*t*-Bu	*t*-Bu	OH	Me
H_2**L2**	*t*-Bu	*t*-Bu	OH	H
H_2**L3**	OMe	CH_2CHCH_2	$O(CH_2CH_2)_2N$	H
H_2**L4**	OMe	Me	$O(CH_2CH_2)_2N$	H

Figure 11. Schematic presentation of the synthesis of polydentate amino- and aminobisphenol ligand precursors.

Suitable stoichiometric amounts of selected phenol, paraformaldehyde and selected amine (2:2:1 for aminobis(phenols), 1:1:1 for aminophenols) were weighed into a small beaker which was placed inside a larger beaker. The large beaker is partially closed with a watch glass and the reaction assembly is placed in a 120°C thermal oven. The reaction vessel is partially closed since some of the starting materials are volatile at these temperatures, and because the evapora-

tion of the water formed is beneficial for the progress of the reaction. The reaction is followed with high-performance liquid chromatography (HPLC); this has proven superior compared to other methods (such as ^{1}H NMR or TLC) since the starting phenols (and possibly also the amine) are usually strongly absorbing in the UV region and thus easily visible with the UV-detector attached to the HPLC instrument. After the reaction has proceeded to the end (judged qualitatively from the amount of the starting phenol) the formed product is purified by recrystallization. If the reaction does not proceed cleanly enough (e.g. there are significant amounts of side products) the desired product can be better separated as a hydrochloride.

The syntheses of the bidentate aminophenols H**L5a-e** (Figure 12) were performed in a fashion similar to preceding ligands. However, since the reactants (mainly secondary amines) do not allow for as many by-products, the reaction times could be increased to improve the yields.

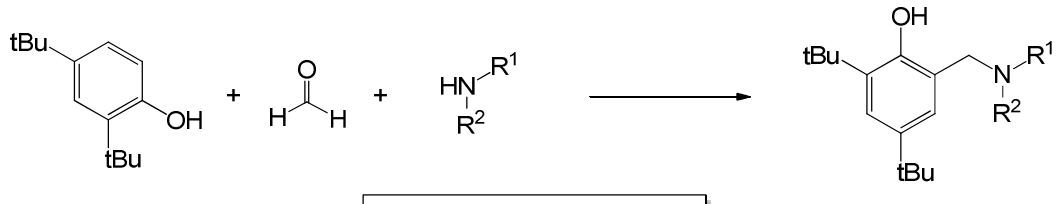

Ligand	R^1	R^2
H**L5a**	H	*i*Pr
H**L5b**	Et	Et
H**L5c**	*i*Pr	*i*Pr
H**L5d**	Me	Ph
H**L5e**	R1-R2 = $(-CH_2-)_5$	

Figure 12. Schematic presentation of the synthesis of bidentate aminophenol ligands.

The potentially tetradentate ligand H_4**L6** was synthesized according to a published synthesis.[5b]

3.2 Complex synthesis

The 3d and 4d transition metal complexes studied in this work were prepared using standard benchtop techniques in the ambient laboratory atmosphere and the reagents and solvents were used as received. For this reason, the screening of large amounts of reactions is more convenient and faster; hence a vast amount of different stoichiometries, solvents and reagents were studied to prepare the desired complexes. Furthermore, for the actual applications, the products should be kinetically and thermodynamically stable with good air and moisture resistance. These generally more feasible properties usually follow from ambient atmosphere synthesis. Because of the more sensitive nature of the starting materials of tungsten complexes ($WOCl_4$ and $WNPhCl_4$),[50] the solvents used in syntheses were freshly distilled over CaH_2 prior to use. The preparation

of the complexes is described briefly and schematically below; see original publications **I-IV** for a more accurate description of the syntheses.

3.2.1 Dinuclear Fe(III) complexes

Three alkoxide-bridged dinuclear Fe(III) complexes were prepared using ligands H_2**L1** or H_2**L2** with stoichiometric amounts of $Fe(acac)_3$ or $FeCl_3$ with modest yields (10-32%), according to the scheme depicted in Figure 13. X-ray diffraction quality crystals of all complexes **1-3** could be separated from the reaction solutions.

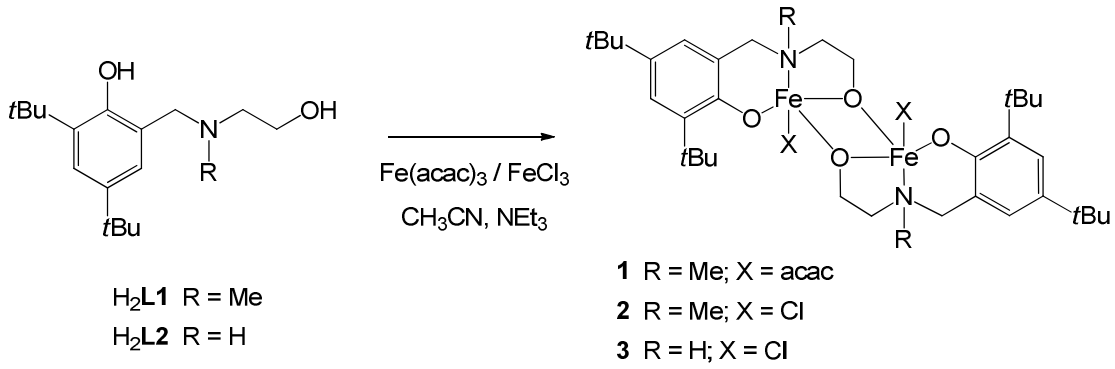

Figure 13. Schematic presentation of the synthesis of the complexes **1-3**.

3.2.2 Mixed-valence Mn(II)/Mn(III) complexes

Six dinuclear alkoxide- or phenoxide-bridged mixed-valence Mn(II)/Mn(III) complexes were prepared using ligands H_2**L3** and H_2**L4** and $MnCl_2{\cdot}4H_2O$ or $MnBr_2{\cdot}4H_2O$ (Figure 14) with good yields (50-76%). The X-ray diffraction quality crystals were mainly grown at room temperature either from the concentrated reaction mixtures or by a slow evaporation of the solutions of the raw products. Substituents R^1 and R^2, the coordinating halide (X) and neutral donor group (D) in Figure 14 of the complexes **4-9** can be found in Table 1.

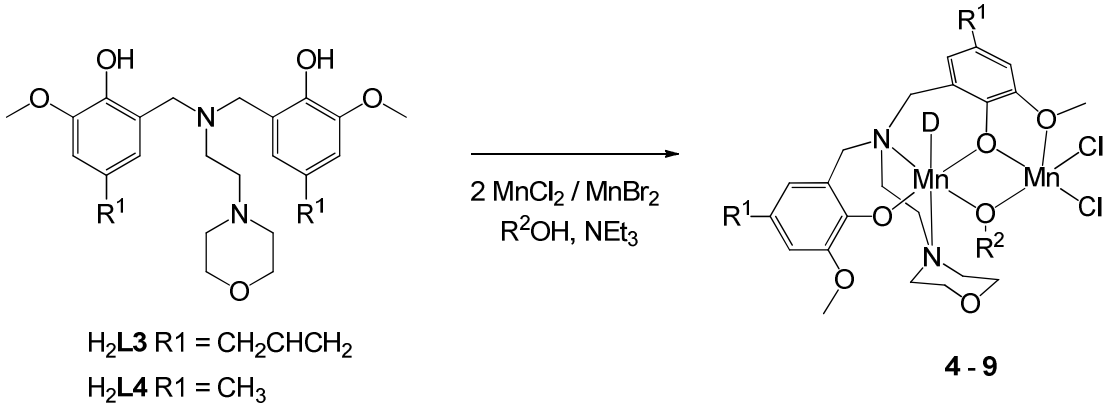

Figure 14. Schematic presentation of the synthesis of complexes **4-9**.

Table 1. Substituents R^1 and R^2, coordinating halide (X) and neutral donor group (D) or bridging group (B) of complexes **4**-**12**.

	R^1	R^2	D/B	X^-
4	CH_2CHCH_2	CH_3	CH_3OH	Cl
5	CH_3	CH_3	CH_3OH	Cl
6	CH_2CHCH_2	CH_3CH_2	CH_3CH_2OH	Cl
7	CH_3	CH_3CH_2	MORPH[a]	Cl
8	CH_2CHCH_2	CH_3	CH_3OH	Br
9	CH_3	CH_3	CH_3OH	Br
10	CH_2CHCH_2	CH_3	CH_3COO^-	-
11	CH_2CHCH_2	CH_3	NO_3^-	-
12	CH_2CHCH_2	-	-	-

[a] The neutral donor of **7** is the morpholine oxygen from a neighboring complex.

The reactivity of complexes **4**-**7** was explored using ammonium and sodium salts of some common anions (NO_3^- and CH_3COO^-) or ethylene glycol as schematized in Figure 15. These reactions produced three additional trinuclear mixed-valence Mn(III)/Mn(II)/Mn(III) complexes (**10**-**12**). See Table 1 for substituents (R^1 and R^2) and the bridging group B. From **10** and **11** only a small amount of single crystals could be separated from the reaction mixtures, while complex **12** could be obtained on a larger scale as X-ray diffraction quality crystals straight from the reaction solution.

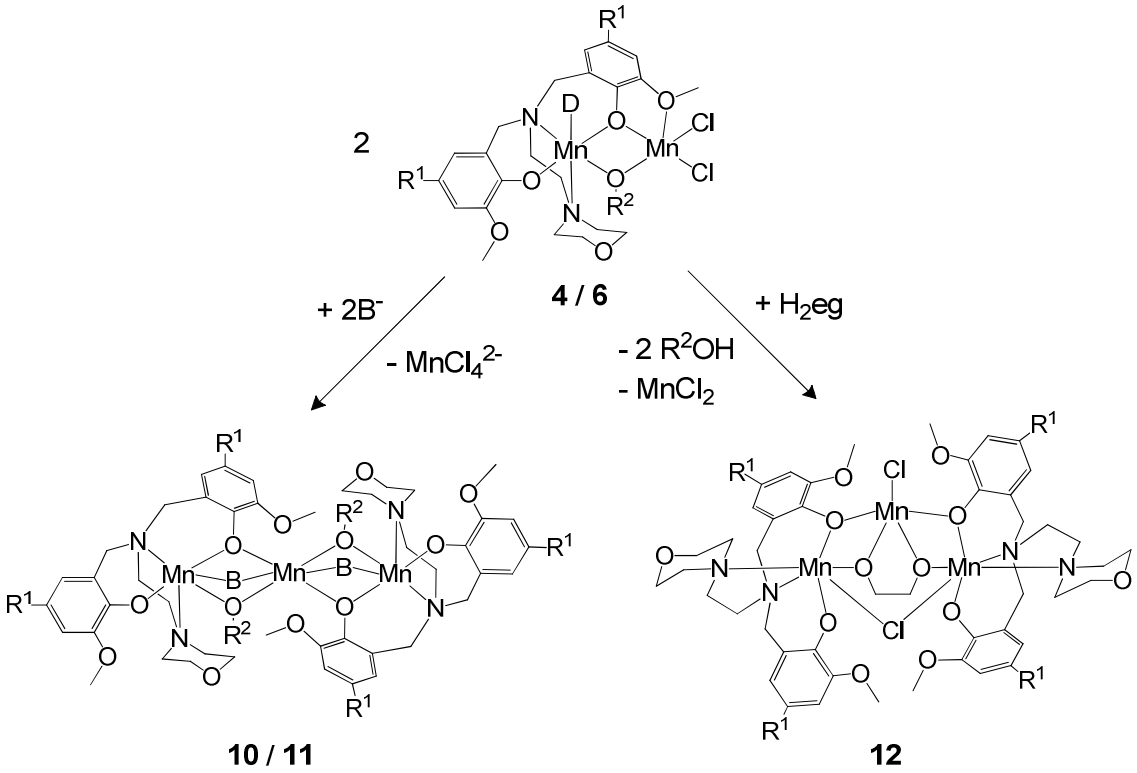

Figure 15. Subsequent reactions performed for complexes **4** and **6**.

3.2.3 Imido W(VI) complexes with bidentate ligands HL5a-e

Two different imido W(VI) complexes were prepared with amino and imino phenolate ligands according to Figure 16. With ligand precursors H**L5b-e** only complex **14** could be separated because of the high reactivity of the initial complexes (see chapter 4.2.1). Single crystals suitable for X-ray diffraction were prepared by re-crystallization of the raw products from hot hexane (**13**) or acetonitrile (**14**).

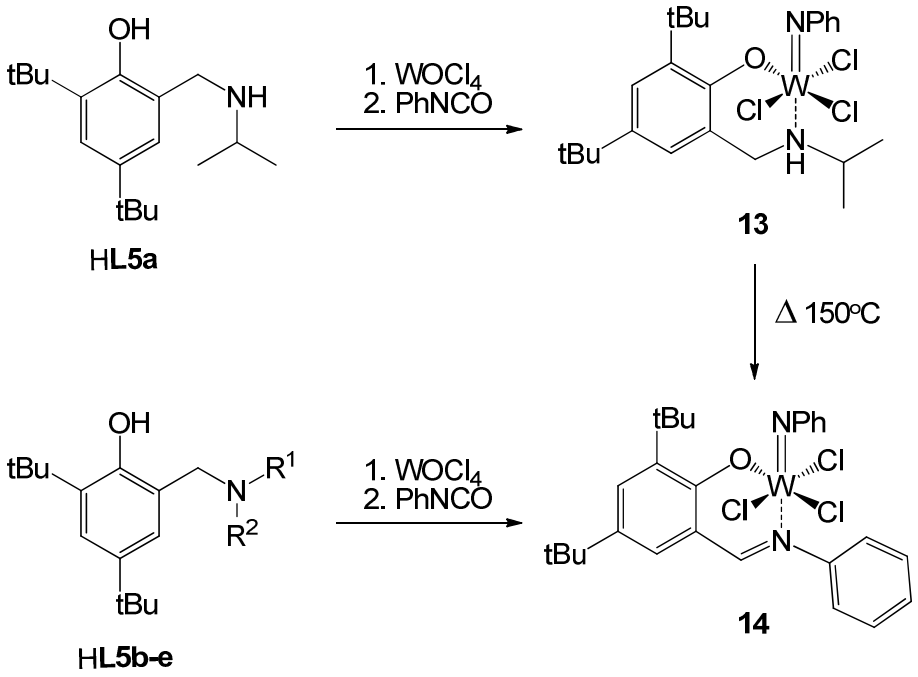

Figure 16. Schematic presentation of the synthesis of complexes **13-14**.

3.2.4 Mo(VI) complexes with non-innocent ligand H_4L6

The complexes **15** and **16** were synthesized as schematized in Figure 17 using potentially tetradentate ligand H_4**L6** and $MoO_2Cl_2(dmf)_2$ of $MoO_2(acac)_2$, respectively. Depending on the metal source and the stoichiometry of the complexation reaction, we were able to separate two entirely different Mo(VI) complexes without any multiply bonded ligands (see Chapter 4.3). From both **15** and **16** X-ray diffraction quality crystals were formed in the reaction mixtures at room temperature.

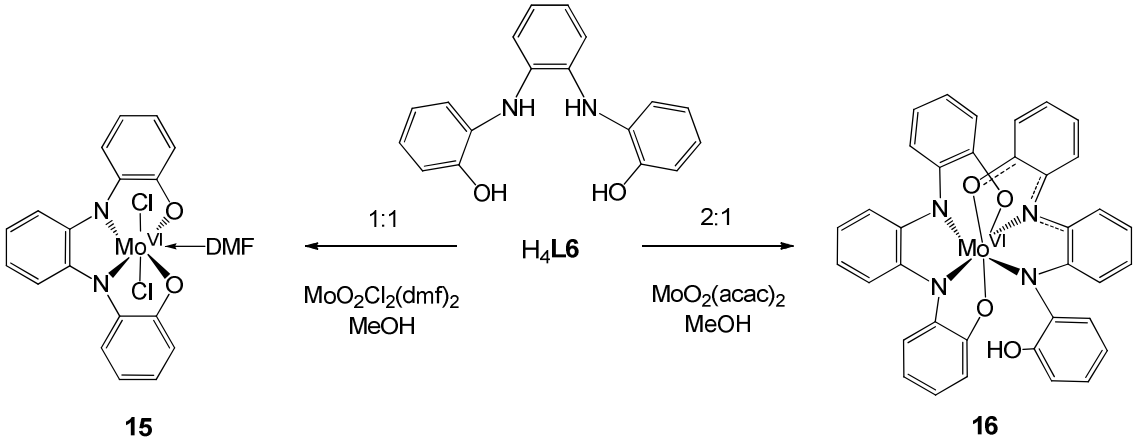

Figure 17. Schematic presentation of the synthesis of complexes **15-16**. *tert*-Butyl substituents of the phenol rings have been omitted for clarity.

3.3 X-ray crystallographic studies

The data collection of all the studied compounds was performed either with an Agilent SuperNova dual wavelength diffractometer equipped with an Atlas CCD area-detector using Cu-K_α radiation, or with a Nonius-Kappa diffractometer equipped with a CCD area-detector using Mo-K_α radiation. For all metal complexes one of the following absorption correction procedures was used: Empirical absorption correction with the SCALE3 ABSPACK scaling algorithm, analytical numeric correction using a multifaceted crystal as implemented in the CrysAlisPro program[51] or the semi-empirical SADABS absorption correction.[52]

The structures were solved by direct methods using the SHELXS-97[53] or the SIR-97[54] program and the full-matrix least-squares refinements on F^2 were performed using the SHELXL-97 program.[53] Figures were drawn with Diamond 3 and Mercury programs.[55] See the original papers for a more accurate description of the crystal structure determinations.

3.4 Computational studies

All theoretical calculations were carried out at the DFT level of theory using either Gaussian 03 or Turbomole 6.3 (6.1 for **III**) program packages.[56] For the exchange coupling constants the calculations were performed on the complexes built from the experimental geometries. The approach used to determine the exchange coupling constants for polynuclear complexes is described in original papers **I** and **II** and references therein. See the original publications for a more complete description of the functionals, basis sets and computational procedures.

4 RESULTS AND DISCUSSION

4.1 Di- and trinuclear 3d complexes with aminophenol and aminobisphenol ligands

The interest towards polynuclear 3d transition metal complexes mostly originates from their common magnetic properties and potential SMM behavior. The molecular structures of all studied complexes were determined by single-crystal X-ray diffraction. A close inspection of the geometrical parameters is required to analyze and identify the important interactions between the paramagnetic centers. Furthermore, information about the exact molecular structure is crucial when modeling the experimentally observed magnetic data. Intramolecular interactions and coordination environment around the metal cations determine the general magnetic behavior of the complexes. However, intermolecular contacts cannot be overlooked since they can often transfer magnetic information between paramagnetic centers, thus affecting the overall properties.

Correlations between certain structural parameters and magnetic behavior in the solid state have already been established with several 3d transition metal complexes. One of the most extensively studied and well-known is the correlation of the magnetic coupling constant (*J*) with the bridging angle of two next-to-nearest Cu(II) cations connected through alkoxide, hydroxide, or phenoxide bridges.[57] Hence, prediction of the magnetic properties of polynuclear metal complexes is possible (to some extent), but it requires combination of extensive experimental and theoretical work to establish the empirical correlations between the nature and magnitude of magnetic interaction and geometrical parameters. However, since the SMM research is still a rapidly developing field, a basic understanding of the relationship between bridging geometry and magnetic properties is of special interest.

4.1.1 Solid-state structures of the complexes

Dinuclear iron(III) complexes

The molecular structure of complexes **1** and **2** is shown in Figure 18 and the relevant bond lengths and angles for all iron(III) complexes are presented in Table 2. The crystal structure of complex **1** consists of neutral [Fe(acac)**L1**]$_2$ molecules of C_i symmetry and a non-coordinating acetonitrile molecule per each dinuclear iron(III) unit. The fully deprotonated tridentate **L1**$^{2-}$ wraps around the metal center, exhibiting a tridentate facial coordination mode with bridging alkoxide oxygen, amine nitrogen and phenoxide oxygen donor atoms leading to a Fe$_2$-(μ-alkoxido)$_2$ rhombus-shaped bridging core. The oxygen donor atoms of the acetylacetonato coligand complete the distorted octahedral FeO$_5$N coordination environment of each iron(III) center. The distortion from an octahedral geometry is mainly caused by the strained 5-membered ring formed by the metal center and the –N-CH$_2$-CH$_2$-O- fragment of the ligand (77.8(1)°), which forces the N8-Fe1-O2^i angle to bend over 25° from the optimal angle of 180°. The Fe-O(acac) bond distances are comparable to those found in other Fe(acac)$_3$ species[58] with a slightly longer Fe-O3 (*trans* to Fe-O1 bond) than Fe-O4 (*trans* to Fe-O2 bond), thus indicating stronger Fe-O(phenolate) bond interactions in comparison to a bridging Fe-O(ethanolate) bond. Overall the Fe-O and Fe-N bond lengths and the Fe-Fe separations are in good agreement with earlier studies.[59]

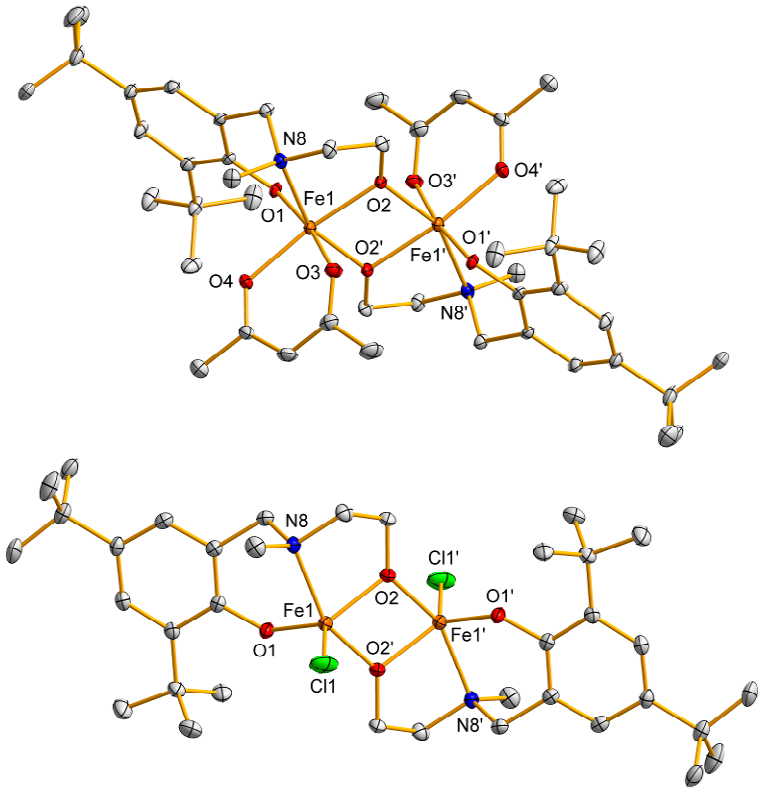

Figure 18. Molecular structures of **1** (top) and **2** (bottom). Thermal ellipsoids have been drawn at the 30% probability level and C-H hydrogens are omitted for clarity. Symmetry codes (') for **1**: 1-x, 1-y, 1-z; **2**: 2-x, 1-y, 2-z;

The solid-state structure of complex **2** contains two halves of distinct dinuclear iron(III) complexes in the asymmetric unit, forming neutral centrosymmetric [FeCl**L1**]$_2$ molecules with slightly different geometries within the unit cell. The amine nitrogens in **2a** and **2b** have dissimilar stereochemistries producing *R* (N8) and *S* (N28) configurations for **2a** and **2b**, respectively. There are few more notable differences in the geometrical parameters around the two different Fe-centers (for example O1-Fe-O2′ and Fe-O2-Fe′ bond angles), but since the coordination spheres and most of the bond lengths and angles are comparable, the structural discussion concentrates on the Fe1-Fe1^{i} centrosymmetric unit depicted in Figure 18.

Table 2. Selected bond lengths(Å) and angles(°) for **1**-**3**. Symmetry codes (′) for **1**: 1-x, 1-y, 1-z; **2a**: 2-x, 1-y, 2-z; **2b**: 1-x, -y, 2-z; **3a**: 1-x, -y, 1-z; **3b**: -x, 1-y, 1-z.

	1	**2a**	**2b**[a]	**3a**	**3b**[a]
Fe1 - Fe1′	3.1311(9)	3.1376(5)	3.1128(6)	3.143(2)	3.125(2)
Fe1 - N8	2.195(3)	2.192(2)	2.179(2)	2.134(7)	2.146(7)
Fe1 - O1	1.901(3)	1.822(2)	1.835(2)	1.831(5)	1.834(5)
Fe1 - O2	2.028(3)	1.955(2)	1.949(2)	1.974(5)	1.948(5)
Fe1 - O2′	1.964(3)	1.997(2)	1.986(2)	1.977(5)	1.969(5)
Fe1 - O3	2.093(3)	-	-	-	-
Fe1 - O3	2.003(3)	-	-	-	-
Fe1 - Cl1	-	2.2155(9)	2.218(1)	2.255(2)	2.237(3)
O1 - Fe1 - O2	102.7(1)	122.04(9)	121.55(9)	119.9(2)	123.9(2)
O2 - Fe - O2′	76.7(1)	74.87(8)	75.46(9)	74.6(2)	74.2(2)
N8 - Fe1 - O2	77.8(1)	78.75(8)	79.51(9)	77.8(2)	79.3(2)
N8 - Fe1 - O2′	154.3(1)	153.19(8)	154.05(9)	152.4(2)	153.3(2)
O1 - Fe1 - O2′	99.1(1)	100.93(9)	96.16(9)	103.5(2)	100.9(2)
Fe1 - O2 - Fe1′	103.3(1)	105.13(9)	104.5(1)	105.4(2)	105.8(2)

[a] The values under **2b** and **3b** are related to the bond parameters around Fe2 in the asymmetric unit.

The ligand **L1**$^{2-}$ settles around the metal ion in the same manner as in complex **1** forming two alkoxide bridges between the iron(III) centers. The chloride ion occupies the vacant site, producing a neutral complex where each iron cation exhibits a five-coordinated $FeNO_3Cl$ coordination sphere with a geometry intermediate between trigonal bipyramidal (TBP) and square pyramidal (SP). To estimate the distortion from TBP to SP, the method of Addison and Rao[60] was used to calculate the δ values for the metal centers. The analysis of the coordination sphere of **2** around Fe1 and Fe2 units gives δ values of 0.54 and 0.52, respectively, which indicate that the geometry is almost at the middle of the TBP-SP deformation pathway. The SP geometry is suggested by the deviation of atom Fe2 from the basal plane formed by atoms O3, O4, O4′ and N28 (0.612 Å) and the presence of the chloride ion at the apical position with a bond distance of 2.218(1) Å. On the other hand, the almost planar O3, O4, Cl2 and Fe2

arrangement and the N28, Fe2, O4' angle of 153.2° support the TBP coordination around the metal center.

The structure forms **3a** and **3b** of complex **3** are quite similar to those of **2** although the methyl group of N8 has been replaced with hydrogen. The asymmetric unit consists of the two halves of the dinuclear iron(III) complexes with the similarly coordinated ligand $\mathbf{L2}^{2-}$. The coordination spheres around iron(III) centers is again an intermediate between TBP and SP geometries (with δ = 0.49 and 0.54 for Fe1 and Fe2, respectively).

In the solid state, the intermolecular interactions of complexes **1–3** are minimal due to the presence of bulky *tert*-butyl substituents in the phenyl rings of the ligands. Thus, neither hydrogen bonds nor π-π interactions are present in the complexes and the interdinuclear Fe···Fe distances are in general over 7 Å.

Mixed-valence Mn(II)/Mn(III) complexes

The molecular structures of all mixed-valence Mn(II)/Mn(III) complexes were determined by single-crystal X-ray diffraction and those of complexes **4** and **6** are presented in Figure 19 (the solid-state structures of compounds **4-5** and **7-9** are similar with only small differences in geometrical parameters, see Table 3). All complexes **4-9** contain six coordinated Mn(III) and five coordinated Mn(II) cations, one aminobis(phenolato) ligand, one bridging alkoxide group and two terminal halides in the same complex unit. The Jahn-Teller distorted Mn(III) ions in all complexes are hexacoordinated with an elongated octahedral coordination sphere, which comprises one coordinated phenoxide oxygen, two tripodal nitrogens, one μ_2-bridging phenoxide group from the ligand and one μ_2-bridging alkoxide oxygen. The sixth coordination site of Mn(III) ions is occupied either by a neutral alcohol molecule (**4-6**, **8** and **9**) or by the morpholine oxygen (**7**) from a neighboring complex. In six coordinated Mn(III) ions O1, N8, O2 and O5 donors form equatorial bonds to the metal ion (1.840 - 2.114 Å), while O6 and N18 form the elongated axial bonds (2.318 – 2.423 Å).

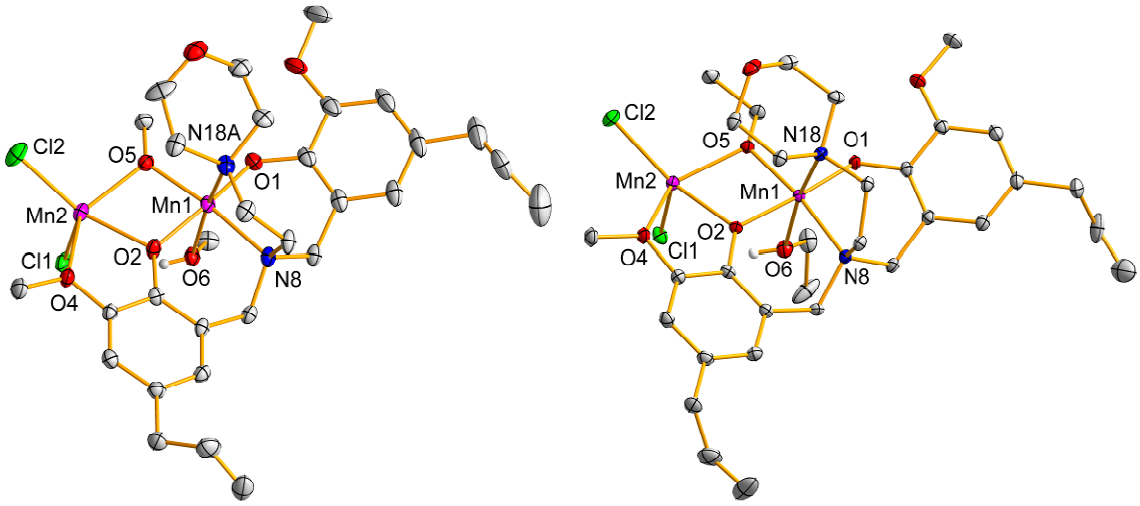

Figure 19. Molecular structures of **4** (left) and **6** (right). Only main components of the disordered morpholine in (**4**) and ethanol in (**6**) are presented. Thermal ellipsoids have been drawn at the 30% probability level and C-H hydrogen atoms are omitted for clarity.

Table 3. Selected bond lengths (Å) and angles (°) of **4**-**9**.

	4	**5**	**6**	**7a**	**7b**	**8**	**9**
Mn1-O1	1.846(2)	1.847(2)	1.857(2)	1.861(5)	1.858(5)	1.840(5)	1.853(4)
Mn1-O2	1.915(2)	1.934(2)	1.903(2)	1.924(5)	1.905(5)	1.912(5)	1.933(4)
Mn1-O5	1.902(2)	1.900(2)	1.912(2)	1.889(6)	1.927(6)	1.902(5)	1.904(4)
Mn1-N8	2.092(3)	2.095(2)	2.090(2)	2.110(7)	2.082(6)	2.114(6)	2.095(5)
Mn1-O6	2.319(2)	2.320(2)	2.323(2)	-	-	2.318(5)	2.329(4)
Mn1-N18	2.413(3)[a]	2.423(2)	2.402(2)	2.357(6)	2.413(6)	2.408(6)	2.411(4)
Mn1-O21'	-	-	-	2.414(5)	2.484(5)	-	-
Mn2-O2	2.109(2)	2.112(2)	2.127(2)	2.160(5)	2.146(6)	2.123(5)	2.100(4)
Mn2-O4	2.433(2)	2.464(2)	2.416(2)	2.422(6)	2.379(6)	2.409(5)	2.476(4)
Mn2-O5	2.127(2)	2.118(2)	2.147(2)	2.152(6)	2.155(6)	2.106(5)	2.115(4)
Mn2-Cl1	2.309(1)	2.338(1)	2.385(1)	2.340(2)	2.349(2)	2.497(2)[b]	2.484(1)[b]
Mn2-Cl2	2.358(1)	2.360(1)	2.326(1)	2.332(2)	2.345(2)	2.480(2)[c]	2.501(1)[c]
Mn1-Mn2	3.1726(6)	3.1777(5)	3.2061(4)	3.2188(16)	3.243(2)	3.1848(15)	3.1733(12)
Mn1-O2-Mn2	104.0(1)	103.4(1)	105.3(1)	103.9(2)	106.2(2)	104.1(2)	103.7(2)
Mn1-O5-Mn2	103.8(1)	104.4(1)	104.2(1)	105.4(2)	105.1(2)	105.1(2)	104.2(2)
Mn1-O2-O5-Mn2	171.8(1)	177.1(1)	171.8(1)	176.5(3)	177.9(3)	175.1(2)	176.5(2)
O2-Mn1-Mn2-O5	169.5(1)	176.2(1)	169.4(1)	175.5(4)	177.2(4)	173.7(3)	175.6(3)
δ[d]	0.09	0.09	0.15	0.12	0.03	0.02	0.07

[a] The nitrogen atoms of the disordered morpholine group have been fixed to the same position (equal Mn-N bond lengths). [b] Mn1-Br1, [c] Mn1-Br2, [d] (β-α)/60, see reference 60.

The pentacoordinated Mn(II) ions have in turn a slightly distorted square-based pyramidal coordination sphere (δ values in Table 3) and they are surrounded by two terminal chlorides (**4**-**7**) or bromides (**8**-**9**), one μ_2-bridging phenoxide oxygen (O2), one μ_2-bridging alkoxide oxygen (O5) and one methoxy oxygen (O4) from the ligand. The other methoxy group (on the side of the hexacoordinated manganese) does not coordinate to a metal cation in any of the complexes studied.

The bond lengths around the manganese atoms in all complexes are comparable with those found in earlier studies concerning similar Mn complexes.[61] The bonds from the Mn(III) ion to phenoxide and alkoxide oxygens are about 0.2 Å shorter than those to the Mn(II) ion from same atoms. This confirms the oxidation state difference between the ions. The Mn1-O1 bond is slightly shorter than the Mn1-O2 one because the O2 acts as a bridge between two manganese ions. In addition, the Mn1-N18 bond is considerably longer (usually by more than 0.3 Å) compared to the other manganese-nitrogen bond (Mn1-N8), which is due to the Jahn-Teller effect of the Mn(III) ion.

The change of the bridging alkoxide group from methoxide (**4**) to ethoxide (**6**) certainly has an influence on the Mn-O5 bond lengths but also on other bonds around manganese cations, which in turn causes variations in the Mn-Mn distance and the Mn-O-Mn angle. Generally the bond lengths between different complexes are similar while the bond angles deviate more. Since com-

plexes **8** and **9** are similar to **4** and **5** with terminal chlorides substituted by bromides, the structural parameters of the corresponding complexes are almost identical (excluding the Mn-X bonds, X=Cl or Br). However, there are small differences in the Mn-O-Mn bond angles between **4** and **8** because of the different packing of the complexes. This is because in complex **8** the coordinated neutral alcohol molecule forms intermolecular hydrogen bonds to neighboring complexes (reminiscent of **5)** instead of the intramolecular ones corresponding t**o 4** with same ligand (**L3**$^{2-}$).

The solid-state ordering of **4**-**6**, **8** or **9** is mainly controlled by inter- or intramolecular hydrogen bonds (Figure 20). These H-bonds can act as transmission pathways for magnetic effects, but the observed magnetic behavior is expected to result from intramolecular coupling of Mn(II) and Mn(III) ions since the magnetic behavior of complexes with different hydrogen bonding patterns is essentially analogous (see below). Conversely, in complex **7** two adjacent complex units are joined together with a quite strong coordinative bond between the Mn(III) ion and the morpholine oxygen. The effects of this coordination on the magnetic behavior of the complexes are discussed in detail later. Furthermore, the unit cells of complexes **4**-**9** do not contain any solvent of crystallization (which could be lost after filtration, thus possibly breaking down the ordering); hence the observed magnetic behavior is explained by the exact geometries determined by single-crystal X-ray diffraction analysis.

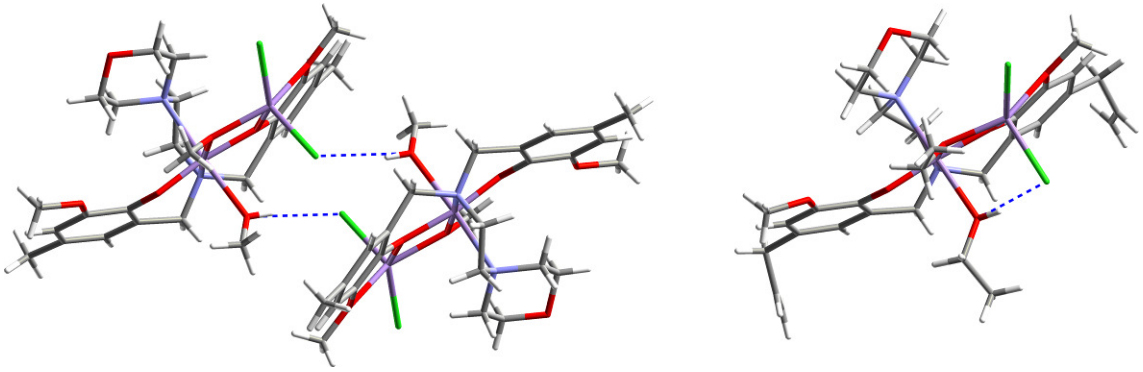

Figure 20. Inter- (left) and intramolecular (right) hydrogen bonding in complexes **5** and **6** respectively.

Products from the subsequent reactions of the Mn(II)/Mn(III) complexes

The reaction of **4** with 2 equivalents of NH_4NO_3 or NaOAc in methanol produced new complexes **10** and **11**. The solid-state structures of these reaction products demonstrate that two bidentate anions (nitrate or acetate) have replaced two chloride anions to produce mixed valence trinuclear Mn(III)/Mn(II)/Mn(III) complexes (Figure 21). Both Mn(III) ions have a distorted octahedral coordination sphere similar to **4** by means of ligand **L3**$^{2-}$ coordinated in a tetradentate manner and a Mn(III)/Mn(II) μ_2-bridging methoxide group. The μ_2-bridging anions have replaced the chlorides, aromatic methoxy substituents and/or coordinated alcohol/morpholine oxygens around the

manganese ions, thus producing a distorted octahedral coordination sphere also for the Mn(II) cation. The donor atoms around the metal ions are identical in both complexes, but the bond lengths and angles around the metal ions are slightly different due to the different nature of the bridging anions (NO_3^- and CH_3COO^-).

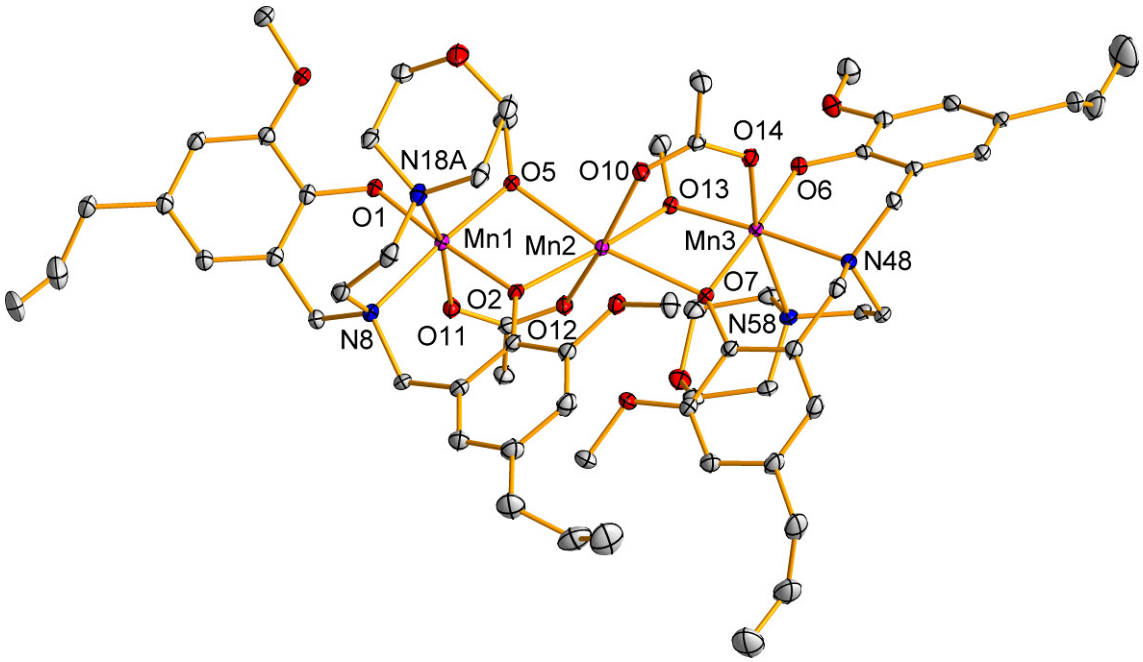

Figure 21. Molecular structure of **11**. Thermal ellipsoids have been drawn at the 30% probability level and C-H hydrogen atoms are omitted for clarity. Only the main part of the disordered morpholine group around N18 is shown.

For complexes **4** and **6**, the reaction between halide and ethylene glycol in acetonitrile produced a new trinuclear mixed-valence Mn(III)/Mn(II)/Mn(III) complex (Figure 22) with a different alkoxide ligand (ethylene glycolate) coordinated to the metal ions. The coordination sphere of both Mn(III) cations is a Jahn-Teller distorted octahedron with a tetradentally coordinated ligand **L3**$^{2-}$, Mn(III)/Mn(II) μ_2-bridging alkoxide oxygens from ethylene glycolate, and an Mn(III)/Mn(III) μ_2-bridging chloride anion vaguely resembling the coordination environment of **4**-**9**. The Mn(II) cation has distorted square pyramidal five-coordination with μ_2-bridging alkoxide and phenoxide oxygens and a terminal chloride anion. The bridging chloride anion between the Mn(III) cations causes the whole structure to be folded (Mn(1)-Cl(2)-Mn(3) angle 111.8°) compared to the rather linear arrangement in **11** and **12**. Selected geometrical parameters of **10**-**12** are presented in Table 4.

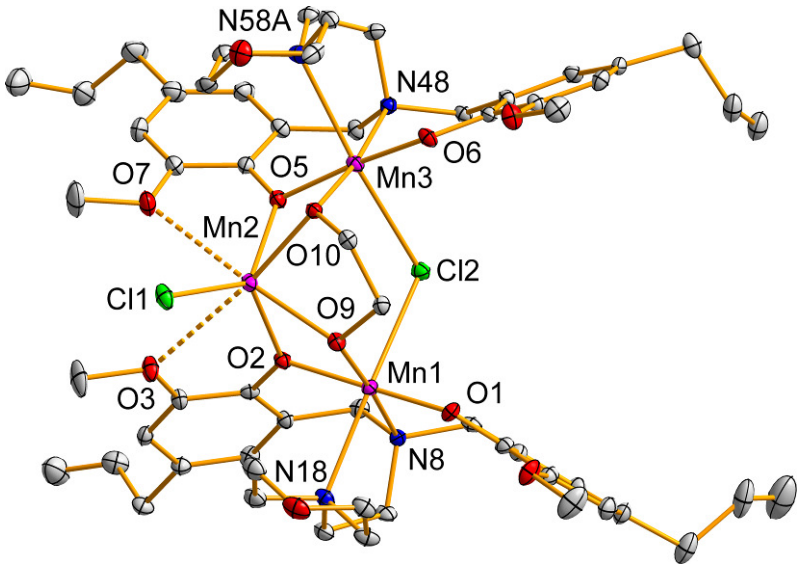

Figure 22. Molecular structure of **12**. Thermal ellipsoids have been drawn at the 30% probability level and hydrogen atoms and non-coordinating solvents are removed for clarity. Only the main part of the disordered morpholine group around N58 is shown.

Table 4. Selected geometrical parameters for complexes **10**-**12**.

	10	**11**		**12**
Mn1-O1	1.876(2)	1.847(4)	Mn1-O1	1.874(3)
Mn1-O2	1.945(2)	1.917(4)	Mn1-O2	1.956(3)
Mn1-O5	1.875(2)	1.875(4)	Mn1-O9	1.884(3)
Mn1-N8	2.091(2)	2.094(4)	Mn1-N8	2.075(4)
Mn1-N18[a]	2.458(2)	2.392(4)	Mn1-N18	2.407(4)
Mn1-O11(O6)[b]	2.220(2)	2.399(3)	Mn1-Cl2	2.635(1)
Mn2-O2	2.236(2)	2.200(4)	Mn2-O2	2.173(3)
Mn2-O5	2.198(1)	2.148(3)	Mn2-O5	2.199(3)
Mn2-O7(O2^{i})	2.271(2)	-	Mn2-O9	2.258(3)
Mn2-O10(O5^{i})	2.205(2)	-	Mn2-O10	2.161(3)
Mn2-O12(O7)	2.140(2)	2.252(4)	Mn2-Cl1	2.372(1)
Mn2-O13(O7^{i})	2.149(2)	-	Mn3-O5	1.927(3)
Mn3-O6(O1^{i})	1.882(2)	-	Mn3-O6	1.842(3)
Mn3-O7(O2^{i})	1.925(2)	-	Mn3-O10	1.885(3)
Mn3-O10(O5^{i})	1.870(2)	-	Mn3-N48	2.069(4)
Mn3-N48(N8^{i})	2.094(2)	-	Mn3-N58[a]	2.472(4)
Mn3-N58(N18^{i})	2.500(2)	-	Mn3-Cl2	2.701(1)
Mn3-O14(O6^{i})	2.193(2)	-	Mn1-O2-Mn2	102.2(1)
Mn1-O2-Mn2	98.89(8)	101.0(2)	Mn1-O9-Mn2	101.5(1)
Mn1-O5-Mn2	102.47(8)	104.3(2)	Mn1-Cl2-Mn3	111.76(4)
Mn2-O7(O2^{i})-Mn3	98.81(8)	-	Mn2-O5-Mn3	100.0(1)
Mn2-O10(O5^{i})-Mn3	103.01(8)	-	Mn2-O10-Mn3	102.8(1)

[a] The morpholine groups in **10** and **12** are disordered but the nitrogen atoms of both parts have been fixed to the same position, hence the Mn-N bond lengths are equal. [b] The atom labels for centrosymmetric complex **11** are presented in parenthesis.

4.1.2 Magnetic properties of the complexes

The magnetic properties of the complexes were investigated experimentally and theoretically to confirm and explicate the results obtained. Initially, the temperature dependence of $\chi_M T$ was measured (χ_M is the molar magnetic susceptibility), from which the nature and magnitude of the exchange coupling (J) between the magnetic ions can be calculated. If ferromagnetic exchange interactions were observed, additional measurements of the field dependence of molar magnetization were performed to extract more information about the intra- and intermolecular magnetic interactions. The presence of magnetic anisotropy was investigated in variable-temperature magnetization experiments and dynamic ac magnetic measurements were performed to figure out if the complexes exhibit slow relaxation of the magnetization and SMM behavior.

Computational analyses at the DFT level were performed to obtain theoretical J values for the complexes, which can be utilized in the analysis of the exchange interactions and to reveal correlations between the magnetic data and the geometrical parameters.

Dinuclear Fe(III) complexes

The temperature dependence of molar magnetic susceptibility ($\chi_M T$) per Fe2 unit for **1–3** was measured in the range of 300–2 K and is shown in Figure 23. The $\chi_M T$ product at room temperature (6.59, 6.29 and 5.9 cm^3mol^{-1} K for **1**, **2** and **3**, respectively) is lower than that expected for two uncoupled S = 5/2 states with g = 2.0 (8.75 cm^3mol^{-1} K), thus indicating the existence of a moderate to strong antiferromagnetic coupling in these compounds.

The χ_M vs. T plots show a wide maximum in the 55-85 K, 80-120 K and 100-125 K range for **1**, **2** and **3**, respectively. Below the temperature of the maximum, χ_M decreases with decreasing temperature and, in the case of **2** and **3**, χ_M increases at a very low temperature, indicating the presence of a small amount of paramagnetic impurity. This behavior suggests antiferromagnetic exchange interaction between the Fe(III) cations leading to an S = 0 ground state. Magnetic susceptibility data were analyzed with the isotropic Hamiltonian $H=-\boldsymbol{H} = -J\boldsymbol{S_1S_2} + g\beta(\boldsymbol{S_1}+\boldsymbol{S_2})H$ and a parameter was included in the theoretical equation to account for the paramagnetic impurity. The best fit of the experimental data to the theoretical equation derived from the above Hamiltonian led to the following parameters: J = –16.1(1) cm^{-1} and g = 2.001(3) for **1**, J = –27.2(5) cm^{-1} and g = 2.15(1) and ρ = 0.003(2) for **2** and J = –29.6(2) cm^{-1} and g = 2.105(4) and ρ = 0.0041(5) for **3**. The J values for **2** and **3** are among the highest found for bis(μ-dialkoxido)diiron(III) complexes.[62]

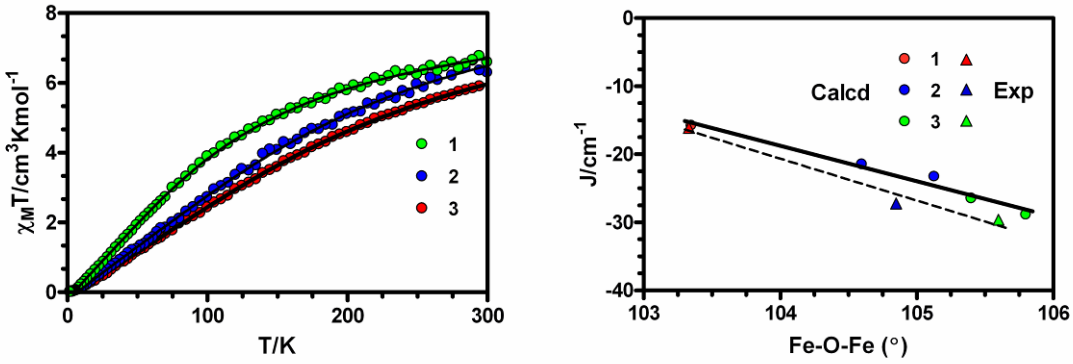

Figure 23. Temperature dependence of $\chi_M T$ for complexes **1-3** (left). Magneto-structural correlations between the exchange coupling constant *J* and the Fe-O-Fe angle (right).

DFT calculations of the magnetic exchange coupling, carried out on the geometries acquired from the crystal structures, predict *J* values for **1-3** (see Table 5) close to those obtained from the experimental susceptibility data. The *J* values were calculated taking into account that the difference between the high-spin state (of multiplicity 11) and the broken-symmetry singlet state is equal to -15*J* .

Table 5. Calculated and experimental *J* values for **1-3**.

	Fe-O-Fe (°)	J_{cal}/cm^{-1}	J_{exp}/cm^{-1}	Fe-O_{av} (Å)	τ (°)
1[a]	103.3	-15.8	-16.1	1.996	21
2a	104.5	-21.5	-27.2	1.968	2.5
2b	105.1	-23.3	-	1.976	14.8
3b	105.5	-26.5	-29.6	1.976	1.9
3a	105.9	-28.9	-	1.959	10.5

[a] Dinuclear units are arranged by the increasing Fe-O-Fe angle.

In complexes **1-3** the magnetic interaction between the Fe(III) cations is mainly governed by the superexchange mechanism through alkoxide bridges involving the $d_{x^2-y^2}/d_{x^2-y^2}$ orbitals (pointing to the direction of the bridging alkoxide ligands) as the most effective pathway mediating the magnetic exchange interaction. Hence, the Fe-O distance and the Fe-O-Fe angle should significantly contribute to the magnetic exchange coupling. In planar $Fe(OR)_2Fe$ complexes, the Fe-O-Fe angle is dependent on the Fe-O bond length (a longer bond indicates a smaller angle) and this is also the case for **1-3** (Table 5); hence there might exist a correlation between one of these structural parameters and the magnetic behavior. Indeed, a strong magneto-structural correlation among the Fe-O-Fe angle and *J* was found with the r^2 value of 0.97 (Figure 23).

These results indicate that for this family of the planar $Fe(OR)_2Fe$ complexes the main structural factor governing the sign and magnitude of the magnetic exchange coupling is the Fe-O-Fe angle. It should be noted that neither the τ angle (the out-of-plane shift of the carbon atom with respect to the $Fe(O)_2Fe$ plane) nor the Fe···Fe distance seems to have a clear influence on the magnetic

exchange coupling. Moreover, as expected from the spherical distribution of the high-spin d^5 ions, the coordination geometry of the iron(III) ions (distorted octahedral for **1** and intermediate between square-pyramidal and trigonal-bipyramidal for **2** and **3**) have no direct effect on *J* either. From the linear correlation between *J* and the Fe-O-Fe angle, the crossover point from AF to F interaction is predicted to be at 100.4° for this family of the ligands. It is important to notice that there also exists a good linear relationship between the experimental *J* values and the Fe-O-Fe angle with $r^2 = 0.97$ and the same cross-over point (Figure 23). It was pointed out earlier that a similar correlation also exists for $Cu(OPh)_2Cu$ complexes, as the main structural factor governing the sign and magnitude of the magnetic exchange coupling is the Cu-O-Cu angle.[57]

Di- and Trinuclear Mn(II)/Mn(III) complexes

The magnetic behavior of mixed-valence Mn(II)/Mn(III) species was studied using complexes **4-9** and **12.** The reactions with NH_4NO_3 and NaOAc did not yield enough products **10** and **11** to perform any other experimental analyses than the structure determination with single-crystal X-ray diffraction (see Chapter 3.2.2).

The magnetic properties of compounds **4-9** and **12** in the form of $\chi_M T$ *vs. T* plots (χ_M being the magnetic susceptibility per $Mn^{II}Mn^{III}$ unit for compounds **4-9**, and per $Mn^{III}Mn^{II}Mn^{III}$ unit for compound **12**) are shown in Figure 24. For **4-9**, the value of $\chi_M T$ at room temperature is slightly higher than the theoretical value (7.375 $cm^3\ mol^{-1}\ K$) expected for a dinuclear system with magnetically isolated Mn^{2+} ($S = 5/2$, $g = 2$) and Mn^{3+} ions ($S = 2$, $g = 2$). When the temperature is lowered, the $\chi_M T$ steadily increases reaching a maximum (a shoulder in the case of **7**) of ~ 12 $cm^3\ mol^{-1}\ K$ at ~10 K. Below this temperature, the $\chi_M T$ decreases rapidly to 2 K (in the case of **7** the $\chi_M T$ sharply increases to reach a value of 16.6 $cm^3\ mol^{-1}\ K$ at 2 K). This behavior is due to a significant intradinuclear ferromagnetic coupling between Mn^{2+} and Mn^{3+} ions leading to an $S = 9/2$ ground state. The decrease in $\chi_M T$ at low temperatures for compounds **4-6** and **9** suggests the existence of zero field splitting effects (ZFS) due to the presence of an anisotropic Mn^{3+} ion (the ZFS for the isotropic Mn^{2+} ion is assumed to be comparatively negligible) and/or intermolecular antiferromagnetic interactions. In the case of **7**, the sharp increase in $\chi_M T$ at low temperature is due to intermolecular ferromagnetic interactions. At room temperature, the $\chi_M T$ value for **12** (11.23 $cm^3 mol^{-1}\ K$) is very close to the expected value for a magnetically uncoupled system containing two Mn^{3+} ions and one Mn^{2+} ion with $g = 2.11$ (11.42 $cm^3 mol^{-1}\ K$). On lowering the temperature, the $\chi_M T$ first decreases slowly until ~100 K and then sharply to reach a value of 4.75 $cm^3 mol^{-1}\ K$ at 2 K. The shape of this curve is typical of a dominant antiferromagnetic coupling in the trinuclear complex **12**. The best fits of the magnetic susceptibility data to the theoretical equation derived from the above Hamiltonian lead to the magnetic parameters gathered in Table 6.

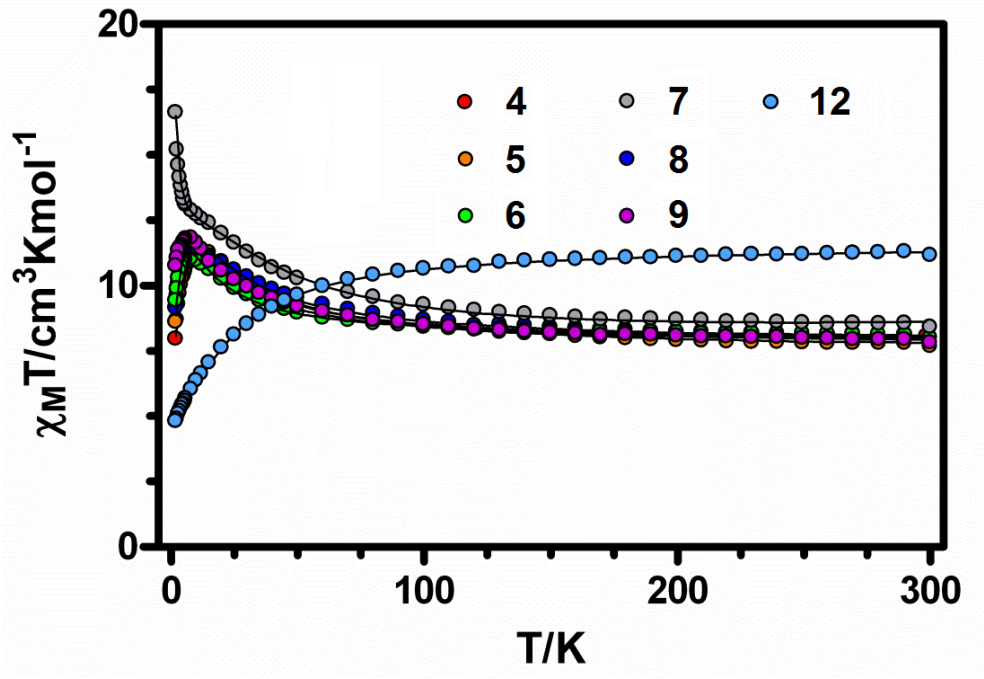

Figure 24. Temperature dependence of the $\chi_M T$ product for complexes **4**-**9** and **12**.

Table 6. Magneto-structural data for the mixed-valence $Mn^{II}Mn^{III}$ complexes **4**-**12**.

Complex	4	5	6	7	8	9	10	11	12
J_{calcd}/ cm^{-1}									
J1-2[a]	+10.4	+13.4	+10.0	+10.7/+12.4[b]	+12.7	+12.6	+5.9	+7.9	+3.1
J2-3 [a]	–	–	–	[b]	–	–	+2.4	+7.9	+0.52
J1-3 [a]	–	–	–	[b]	–	–	−0.37	−0.44	−8.6
J1-4 [a]	–	–	–	[b]	–	–	–	–	–
J_{exp}/ cm^{-1}									
J1-2 (J1′-2′)	+3.44(6)	+4.2(1)	+2.15(6)	+7.9(7)	+3.7(1)	+2.9(1)	–	–	0.04(7)
J2-2′							–	–	-5.3(1)
g	2.045(2)	2.012(4)	2.032(3)	1.993(1)	2.049(5)	2.042(3)	–	–	2.11(1)
zJ′	-0.10(1)	-0.06(1)	-0.07(1)	-0.04(1)	-0.08(1)	-0.04(1)	–	–	–
θ/(°)[c]	103.88	103.90	104.73	105.15	104.61	103.93	100.68	102.65	101.63
d /(Å)[d]	3.179	3.178	3.206	3.231	3.185	3.173	3.189	3.181	3.191
(δ, %)[e]	9.3	7.2	14.4	2.4/11.7	2.3	6.8	–	–	17.3

[a] Numbers correspond to the crystallographic numbering of Mn cations. [b] The pair of values refers to both dinuclear subunits forming the tetranuclear complex, the other coupling values being very small. [c] Mn-O-Mn angle, average value [d] Mn(II)-Mn(III) distance, average value for **7**, **10** and **12** [e] Distortion from SPY-5 toward TPBY-5 (δ) calculated using Addison's method: δ =(β-α)/60; α and β are the largest *trans* bond angles, see reference 60.

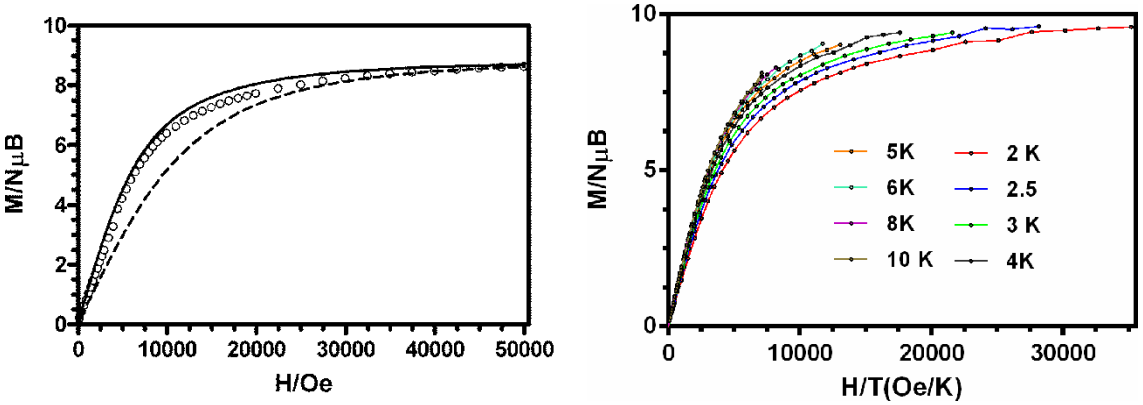

Figure 25. M vs. H plot for **6**. The solid and dashed lines represent the Brillouin functions for an $S = 9/2$ ground state and for the sum of an $S = 2$ and an $S = 5/2$ spin states with g = 2.03, respectively (left), and *M vs. H/T* plots for **6**. Solid lines are guides for the eye (right).

The field dependences of the molar magnetization at 2 K for compounds **4**-**9** (the *M* vs. H plot for compound **6** is given as an example in Figure 25) are below the Brillouin function for $S = 9/2$, which is likely due to the combined effects of interdimer antiferromagnetic interactions and/or zero-field splitting of the $S = 9/2$ ground state. However, the experimental values are well above the sum of the magnetization contributions expected for the isolated ions, thus supporting the presence of intramolecular ferromagnetic interaction in these compounds.

Variable-temperature magnetization data were collected between 2 and 10 K at applied fields ranging from 0.5 to 7 T. The *M* vs. *H*/*T* plots for **4**-**9** (the plot for compound **6** is given as an example in Figure 25) do not follow a single master curve, clearly indicating the presence of a significant magnetic anisotropy in these complexes. However, all attempts to obtain the *D* and *E* anisotropic parameters of the $S = 9/2$ ground state by fitting the reduced magnetization data were unsuccessful.

The sign and magnitude of the ferromagnetic exchange interactions in $Mn^{II}Mn^{III}$ mixed-valence pairs can be explicated using the known Goodenough–Kanamori rules and spin-polarization mechanism (see Chapter 2.1.1).[22] In addition, the magnetic coupling might also contain a contribution from a double-exchange (also known as spin-dependent delocalization) mechanism, which is always positive (ferromagnetic).[63] While the superexchange takes place by electron transfer via an excited state mixed into the ground state by second-order perturbation, the double exchange occurs via ground-state configurations. However, in complexes **4**-**9**, the double-exchange term is expected to be very small, as the valences of the Mn^{2+} and Mn^{3+} are essentially trapped (class I compounds according to the Robin and Day classification).

The experimental magnetic data and a detailed orbital examination supported by a literature review suggest that the planar $Mn(II)(O)_2Mn(III)$ bridging fragment with a relatively large Mn-O-Mn angle (> 100°) favors the ferromagnetic contributions between the magnetic orbitals of the manganese cations, thus inducing ferromagnetic coupling, in all dinuclear complexes studied. Fur-

thermore, the lack of distortion in the Mn(II) cation from the ideal square pyramidal geometry (δ) seems to enhance the magnetic coupling, thus producing larger J values. These hypotheses were consolidated with comprehensive DFT calculations performed for model compounds (Figure 26).[II]

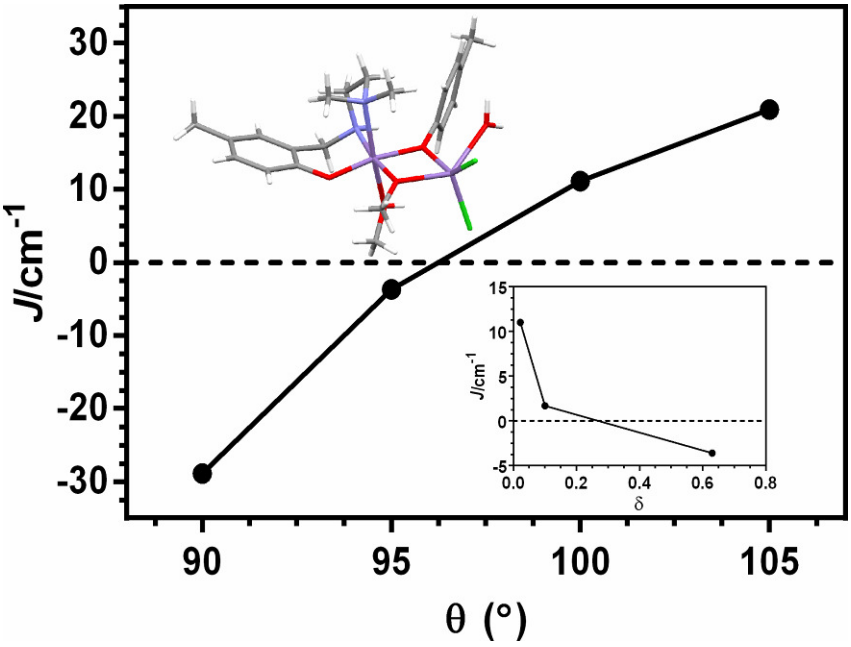

Figure 26. Calculated J values *vs.* the Mn^{2+}–O–Mn^{3+} angle (θ) and calculated J values *vs.* δ (inset) for the model compound (depicted in the top left corner of the figure).

In conclusion, the Fe(III) and Mn(II/III) complexes presented above demonstrate the possibilities and performance of polydentate aminophenolate ligands in the synthesis of di- and trinuclear 3d metal complexes. The experimental and computational investigation of **1-12** addresses definite correlations between certain structural parameters and the magnetic behavior of the compounds. While the relatively small number of examples prevents universal conclusions, these results clearly indicate that meaningful magnetostructural correlations can be formed in this type of iron and manganese complexes.

4.2 Imidotungsten(VI) complexes with chelating amino and imino phenolates

In addition to polynuclear metal complexes, the aminophenol ligand framework can be utilized in the synthesis of mononuclear species which are frequently used, for example, in homogenous catalysis or other metal mediated chemical transformations. Imidotungsten(VI) complexes with aminophenolate ligands have shown some catalytic performance in certain ROMP reactions, although there is still room for improvement.[64] The relatively poor catalytic be-

havior can be hypothesized to originate from rather strong coordinative W-N_{amine} bonds. On the other hand, the stability of the complexes is also relative to this bond since the aminophenolate ligands lose the benefits of the chelate effect when this bond is broken. In previous studies, some difficulties have appeared in isolating the aminophenolate complexes of the W(VI) cation; hence we have studied the nature of the crucial W-N_{amine} bond by experimental and computational methods.

4.2.1 Synthesis, reactivity and structural characterization of imidotungsten(VI) aminophenolate complex

The imidotungsten(VI) complex **13** was prepared in a simple two-step one-pot reaction. The first step comprises a stoichiometric reaction of aminophenol ligand H**L5a** (see Chapter 3.1) and oxotungsten(VI) tetrachloride ($WOCl_4$) in dichloromethane. The second step involves the reaction of the prepared tungsten oxo complex with phenyl isocyanate in toluene producing the desired complex. The complex can be crystallized as X-ray diffraction quality crystals from the toluene-hexane mixture.

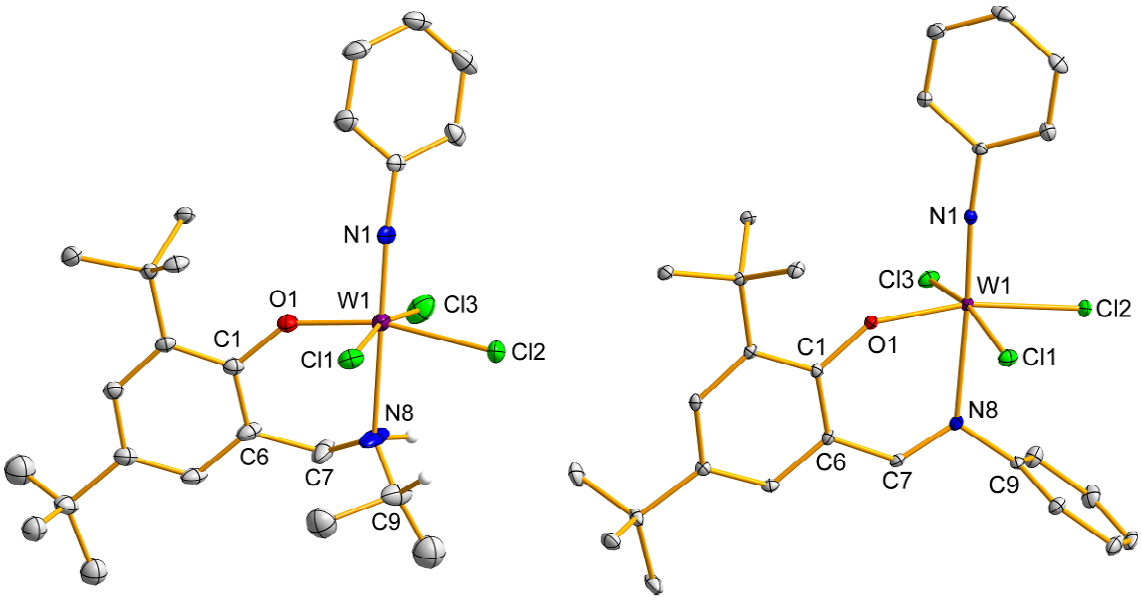

Figure 27. Molecular structures of aminophenolate complex **13** (left) and Schiff-base complex **14** (right). For **13** only the main component of the disordered *tert*-butyl group is presented. Thermal ellipsoids have been drawn at the 20% probability level and most of the C-H hydrogen atoms are omitted for clarity.

The molecular structure of **13** consists of neutral mononuclear units, in which the central W(VI) ion is surrounded by one terminal phenyl imido group, one bidentate aminophenolate and three chlorides (Figure 27). As expected due to the strong structural *trans*-effect of the imido nitrogen,[65] the neutral donor atom of an aminophenolate is situated *trans* to the imido group. The coordination geometry and bonding parameters (Table 7) around the metal ion are comparable to those found earlier for the corresponding aminophenolate com-

pounds.[64,66] As expected from theoretical calculations (see below), the observed coordinative W–N bond length in **13** is rather short (2.339 Å).

Table 7. Selected bond lengths (Å) and angles (°) for **13** and **14**.

	13	**14**
W1-N1	1.723(7)	1.712(7)
W1-N8	2.339(8)	2.329(8)
W1-O1	1.870(6)	1.868(6)
W1-Cl1	2.347(3)	2.359(2)
W1-Cl2	2.371(2)	2.3232(9)
W1-Cl3	2.370(3)	2.3630(10)
N1-W1-N8	171.9(4)	173.8(4)
W1-O1-C1	145.22(19)	143.1(5)
N1-W1-O1	98.6(3)	96.4(3)

The solution-state structure of **13** was verified by NMR measurements with the help of standard 2D NMR experiments. According to the analysis, the coordinative W1-N8 bond seems to remain intact in the $CDCl_3$ solution. Nevertheless, the solution-state structure appears not to resemble the solid-state structure of **13;** the data better corresponds to a C1-C6-C7-N8-W1-O1 ring inversed conformation. This is in a good agreement with the thermal motion of the amino group observed in the crystal structure. In addition, the ^{15}N chemical shifts of the amino-type NH and imido nitrogens are consistent with the sp^3 and sp^2 hybridization, respectively, which further supports the conclusion that the complex is stable in solution (at room temperature).

The two-step reactions with ligands H**L5b-e** (Chapter 3.1) with $WOCl_4$ were carried out as described above for H**L5a**. However, these experimental conditions did not produce the expected aminophenol complex, but the reaction led to the formation of a deep purple solution from which an intense purple compound **14** was obtained as the only isolable product. The X-ray crystallography showed the formation of a rare example of an imidotungsten(VI) complex with Schiff-base ligand.[67] The structure consists of neutral mononuclear units in which the central W(VI) ion is surrounded by one terminal phenyl imido group, one bidentate iminophenolate ligand and three chlorides. In general, complex **14** has a coordination sphere around the metal center rather similar to that in aminophenolate complex **13** (see Table 7 and Figure 27). The neutral imine nitrogen is bonded *trans* to the phenylimido group, the N-W═N angle being 173.8(4)°. The NMR data indicate that the solid-state structure is retained in a $CDCl_3$ solution, as the coordinative bond between W1 and N8 remains intact. As estimated from computational results (see below), the coordinative W–N(imino) bond length in **14** is relatively long (2.329(8) Å), whereas the related bond lengths are 2.308 Å in $[W(N\textit{t}Bu)_2L]$ (L is a dianion of N,N-bis(3,5-di-tert-butylsalicylidene)ethane-1,2-diamine, the neutral imine nitrogen being *trans* to the imido dianion) and 2.234 Å in $[WO_2(L')(MeOH)]\cdot MeOH$ (L′ = 2-(salicylideneamino)-5-t-butylphenolate dianion, the neutral imine nitrogen being *trans* to the oxo group).[67a,68]

The Schiff-base complex **14** is also formed in the reaction of $W(NPh)Cl_4$ with ligand precursors H**L5b–e** in refluxing toluene, indicating that phenyl isocyanate is not required in the formation of the new Schiff-base ligand, but the imino group in this new ligand comes from the W=NPh functionality. The mechanism of this reaction is so far unclear, though formally it appears to be a disproportionation of an intermediate compound analogous to complex **13**. The weak coordination ability of the amino group in phenols H**L5b–e** obviously has an essential role in this reactivity. To have more evidence on this disproportionation, the thermal decomposition of well-characterized aminophenolate complexes was investigated. Isolated compounds **13** and $[W(NPh)Cl_3(OC_6H_3(CH_2NMe_2)\text{-}2\text{-}t\text{-}Bu_2\text{-}4,6)]$[66b] are stable in toluene under reflux temperature, but if they are heated in 1,2-dichlorobenzene at 150 °C, the above mentioned Schiff-base complex **14** is formed in a 35% isolated yield. The higher stability of these complexes is consistent with the observed and calculated coordinative W–N distances (Table 8).

4.2.2 W-N bond analysis

The factors contributing to the bond strength between the tungsten(VI) ion and the amine nitrogen are the sterical hindrance induced by alkyl substituents, the inductive effect and the resonance effect. To study the influence of these effects on the coordinative W-N bond, geometry optimizations (at the DFT BP86/def2-TZVP level) and partial atomic charge calculations were performed on a group of simplified model complexes of imidotungsten(VI) trichloride with different aminophenolate ligands (Figure 28).

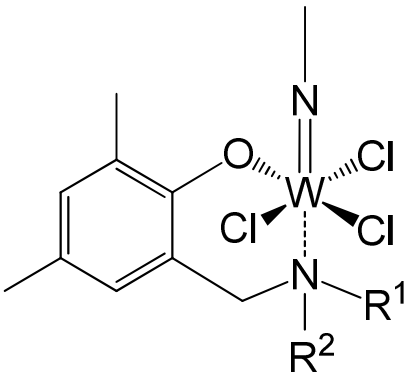

Figure 28. Schematic presentation of simplified model complexes**.**

The amine ligands in the model complexes can be divided into primary (entry 1 in Table 8), secondary (entries 2-4) and tertiary amines (entries 5-7). Furthermore, the geometries of two related Schiff-base complexes (entries 8–9) were optimized, although their bonding mode is differs from that of the aminophenolate complexes. In these models, the C=N double bond may provide additional electrons by π-donation to the W–N bond, thus shortening the bonding distance and increasing the stability of the Schiff-base complexes.

The effect of the alkyl group on the W-N_{amine} bond can be clearly seen from the calculated data, *i.e.*, the bond length increases upon the size of the substituents. The most significant result from the theoretical study is the notable shortening of the W-N_{amine} bond in the complexes with secondary amines compared to the more common tertiary amine complexes. In general, the calculated W-N_{amine} bond lengths in secondary amine complexes are from 0.2 to 0.6 Å shorter than those in corresponding tertiary amines. The calculated bond lengths are in good agreement with the experimental data where available. The small differences between the theoretical and experimental results (approximately 0.1 Å) in the W-N_{amine} bond distances are most likely due to solid-state packing effects, which are not taken into account in the calculations.

Table 8. Calculated W-N bond lengths, MPA and NPA charges for the N donors and ϕ angles of model complexes.

Entry	R_1	R_2	r (W-N) Å	Q (MPA)	Q(NPA)	ϕ °
1	H	H	2.38	-0.800	-0.459	38.9
2	H	Me	2.44	-0.601	-0.335	38.2
3	H	Et	2.46	-0.609	-0.306	39.1
4	H	iPr	2.47	-0.619	-0.317	37.9
5	Me	Me	2.60	-0.407	-0.232	37.2
6	Et	Et	2.68	-0.411	-0.205	35.8
7	iPr	iPr	3.06	-0.416	-0.184	34.7
8	Me	–	2.38	-0.424	-0.155	–
9	Ph	–	2.41	-0.442	-0.210	–

In order to explain this trend, the atomic charges were calculated for all studied complexes. Although the computational partial atomic charges can be rather arbitrary models, they still provide useful and chemically interpretable information about the properties of the molecules. Hence, the Mulliken population analysis (MPA) and the Natural Population Analysis (NPA) were performed for the preceding model compounds (see Table 8). According to the extensive study by Hadad *et al.* on the competence of different atomic charge schemes, NPA gives truthful charges of the nitrogen atoms in substituted anilines.[69] Consequently, the NPA analysis was at least assumed to provide reasonable results about the partial atomic charges of the amine complexes as well.

The electron-releasing ability of the nitrogen substituents follows the order H > $CHMe_2$ > CH_2Me > CH_3 according to the calculated MPA charges. A similar trend can be also found in the NPA charges, although some inconsistency is observed. However, both methods predict the nitrogen donors' partial charge to be substantially more negative in the primary and secondary amines than in the tertiary ones. This trend is in line with the calculated and experimentally observed W-N bond lengths, as the bond length decreases when the negative partial charge of nitrogen increases. Since the partial atomic charge of tungsten remains in practice at the same level through the whole series, the charge difference between tungsten and nitrogen atoms increases, thus adding to the attractive electrostatic contribution of the bond.

In addition to the partial charge of the nitrogen donor, there exists a correlation of the calculated W-N bond lengths with the pyramidality (the dihedral angle CH_2-R1-R2-N, Φ) of the nitrogen atom. The pyramidality of a nitrogen atom indicates the steric hindrance of the donor group. Hence, the more pyramidalized (*i.e.* the larger the Φ angle), the better donor the nitrogen atom can be.

To conclude, the ligands H**L5a-e** can be seen as structurally non-innocent (undergoing a chemical transformation during/after coordination to a metal cation) ligands as they undergo a C-N bond cleavage with the following imino bond formation during the complexation reaction (H**L5b-e**) or at elevated temperatures (H**L5a**). The formed Schiff-base ligand could be easily synthesized in a condensation reaction between substituted 2-hydroxybenzaldehyde and aniline separately from the imidotungsten(VI) fragment. However, substituted hydroxybenzaldehydes are very expensive compared to substituted phenols (starting material for the ligands H**L5a-e**); hence the above reactivity could be exploited in the synthesis of novel Schiff-base ligands.

4.3 Mo(VI) complexes with non-innocent phenylenediamine bis(phenolate) ligand

The combination of the redox-active nature of ligand H_4**L6** (see Chapter 3.1) and the reactivity of the MoO_2^{2+} functionality could generate new potential oxotransfer catalysts. Hence the reaction of this ligand with several MoO_2^{2+} sources was studied to obtain novel mononuclear Mo(VI) complexes. However, none of the reactions studied did yield the desired oxidomolybdenum(VI) complex because the terminal oxido groups of the molybdenyl ion were removed upon the ligand coordination, and two new molybdenum complexes with ligand H_4**L6** were formed. The syntheses, molecular structures and magnetic behavior of these complexes are described and discussed below. The heptacoordinated complexes [Mo^{VI}(**L6**)Cl_2(dmf)] (**15**) and [Mo^{VI}(**L6**)(H**L6**)] (**16**) are of interest due to their general coordination chemistry and the non-innocent behavior of the ligand. In support of the experimental work, a comprehensive computational study was carried out to address the electronic nature of compounds **15** and **16**.

4.3.1 Structural studies

Crystals of **15** were obtained from the reaction mixture in acetonitrile. In the solid state (Figure 29), the molybdenum atom shares a plane with two oxygen atoms and two nitrogen atoms from the **L6**$^{4-}$ ligand, as well as with one oxygen donor from the coordinated dmf ligand. Two chlorides in axial positions complete the heptacoordinated environment around the metal center, which is best described as a distorted pentagonal bipyramid.[70] In principle, the protonation and oxidation level of the $H_4N_2O_2$ ligand can be determined from high-quality single-crystal X-ray data, as the C-C, C-N and C-O distances change sys-

tematically upon stepwise one-electron oxidation processes. In **15**, the C-C bond lengths within both the phenolic parts of the N_2O_2 ligand and the central ring fall in the range 1.376(3) – 1.411(3) Å (see Table 9 below), which does not allow an unambiguous definition of the oxidation state of the ligand. Similarly, the C-N and C-O bond distances of 1.398(3) Å and 1.322(2) Å, respectively, indicate that the ligand oxidation state might be either -1 or -2, while the observed metal-to-donor-atom distances are characteristic for anionic phenoxide and amide ligands. Consequently, theoretical calculations at the DFT level were performed for a model system of **15** (see below).

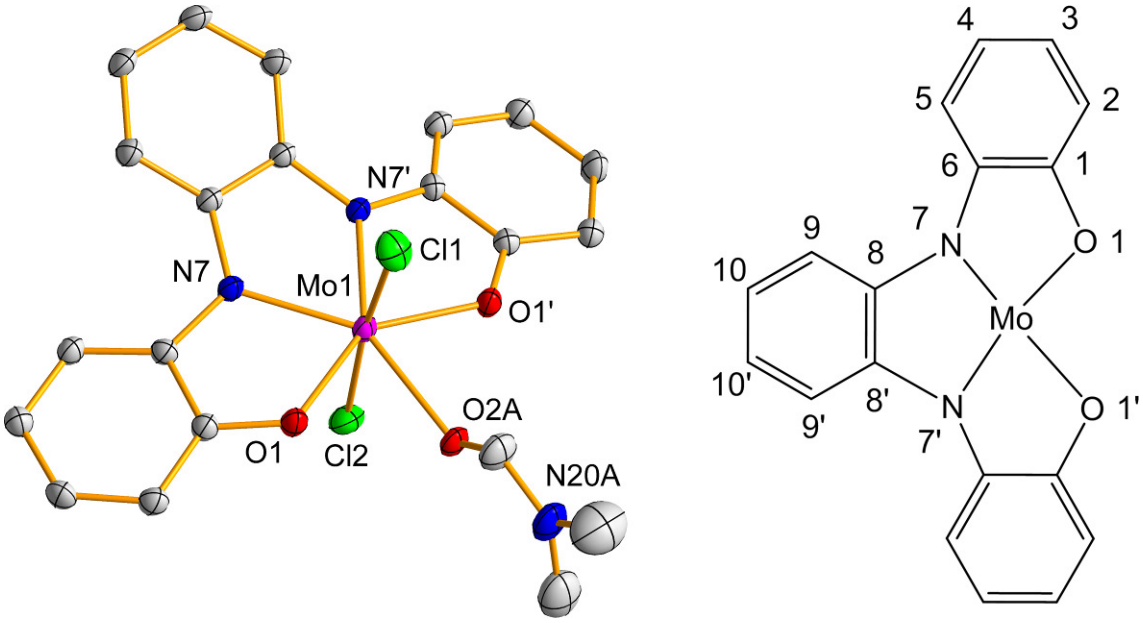

Figure 29. Crystal structure of **15** (left) and its numbering scheme (right). Symmetry operation ' = x, 0.5-y, z. CH hydrogens, *tert*-butyl substituents and other parts of the disordered dmf molecule are omitted for clarity. Thermal ellipsoids are drawn at the 30% probability level.

Single crystals of **16** were separated from the methanol solution of the ligand and and $[Mo^{VI}O_2(acac)_2]$ as described above. The X-ray structure (Figure 30) showed that the asymmetric unit consists of two crystallographically independent molecules with comparable structural parameters (see below). In these molecules, both the oxido moieties and the acetylacetonato ligands have been replaced during complexation, the final product being a neutral heptacoordinated complex $[Mo^{VI}(\mathbf{L6})(H\mathbf{L6})]$, where the ligand displays two different coordination modes. One of the two ligands is fully deprotonated, whereas the other ligand has a dangling phenol part with an intact OH group (H**L6**). Similarly to complex **15**, the ligand assembly is not unambiguous, since the quality of the X-ray data does not allow an in-depth analysis of the geometrical parameters. Nevertheless, the tetradentate ligand $\mathbf{L6}^{4-}$ seems to be analogous to a fully deprotonated one as in **15**, whereas the tridentate ligand with a dangling phenol part can be best described as a triply deprotonated ligand $[H\mathbf{L6}^{\bullet}]^{2-}$. With these presumptions, the formal oxidation state of the metal center is Mo(VI). As the oxi-

dation level assumed for the tridentate ligand involves one unpaired electron, the material should be paramagnetic.

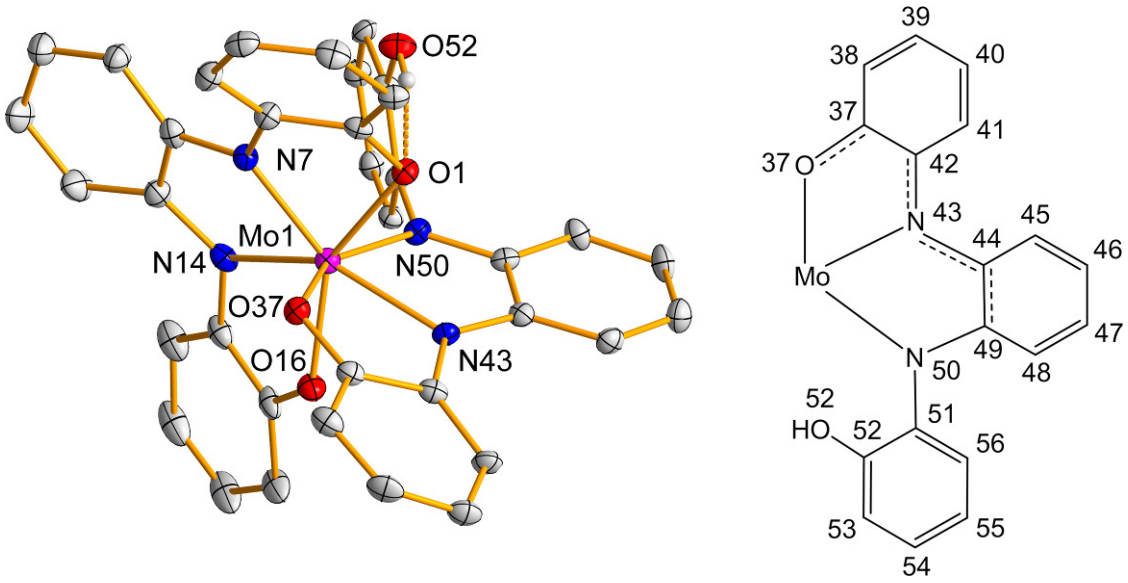

Figure 30. Crystal structure of **16** (left) and its second ligand's numbering scheme (right). CH hydrogens and *tert*-butyl substituents are omitted for clarity. Thermal ellipsoids are drawn at the 30% probability level.

4.3.2 Magnetic properties and ESR

Compound **15** showed only diamagnetic behavior, as expected due to the even number of electrons. Compound **16**, on the other hand, gave a paramagnetic signal with a susceptibility χ_{mol} = 4.2×10^{-7} m^3/mol at 5 K ($\chi_{mol} = M \cdot \chi_v / \rho$, where ρ is the density, M is molar mass and χ_v is volume magnetic susceptibility). The temperature dependence of the susceptibility was also measured and the data were fitted to the Curie-law of localized moments, $\chi_{mol} = C/(T-\theta_p)$. Figure 31 shows the χ_{mol} *vs.* T and $1/\chi_{mol}$ *vs.* T plots of **16**. As can be seen from the figure, the inverse of susceptibility does not obey the Curie law, which means that the magnetic spin is not localized. However, χ_{mol} is not temperature-independent either, as would be expected for Pauli paramagnetism induced by a completely non-localized electron. Consequently, the most probable explanation of the data measured for compound **16** is a partially localized unpaired electron that is causing the magnetic properties.[71] The calculated magnetic moment (μ_{eff}) at the high temperature range (T > 150 K) is 1.80 B.M. whereas it is 1.25 B.M. at the low temperature range (T < 80 K). As the 'spin only' value for an unpaired electron is 1.73 B.M., the magnetic moment in the high temperature range clearly indicates the presence of only one unpaired electron.

X-band electron spin resonance (ESR) spectra of solid compounds **15** and **16** were measured at room temperature as well as at 4 K, while the solution spectrum of **16** was measured in CH_2Cl_2 at room temperature. As expected, compound **15** did not show an ESR signal, while a solid sample of **16** gave an axial spectrum at 4 K with $g_\perp$ = 2.0157 and $g_{||}$ = 2.0047 (Figure 32). Thus, the

calculated Δg = 0.011 and <g> = 2.012. In CH_2Cl_2, **16** produced a nearly isotropic ESR signal (S=½) g_{iso} = 2.0087 with a minor asymmetry, possibly due to an unresolved hyperfine interaction. These values clearly indicate that the unpaired electron is predominantly on the orbitals of the ligand, in a similar fashion as in Ni(II) and Ru(II) semiquinone complexes,[72] and not on the metal because <g> can vary from 1.938 to 1.952 as reported earlier for octahedral Mo(V) compounds.[73] Against this scenario, **16** is best described as a molybdenum(VI) complex with a semiquinone-type radical ligand.

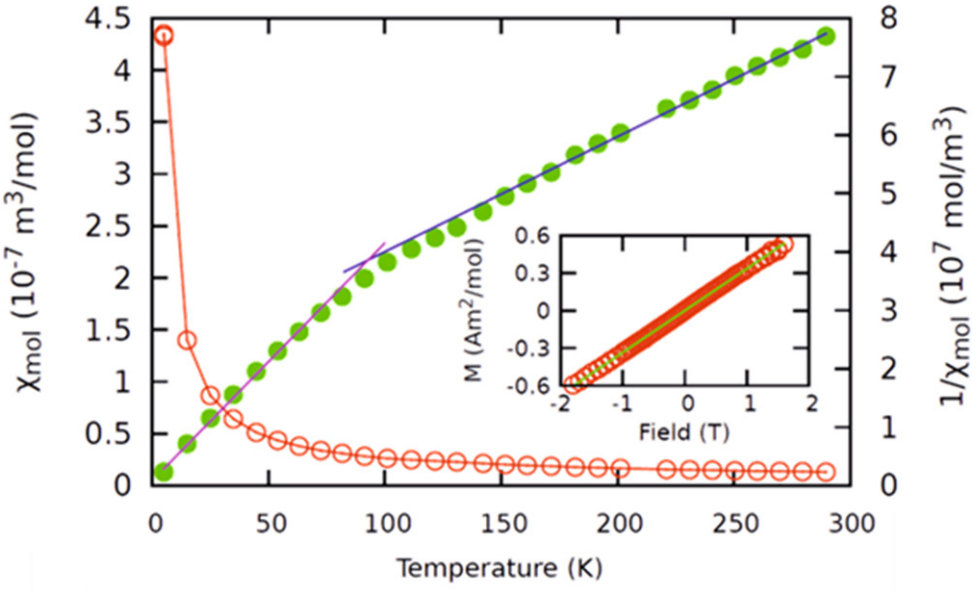

Figure 31. Plot of susceptibility $\chi_{mol}T$ *vs.* T of compound **16** in a 0.1 T field. The green dotted values show $1/\chi_{mol}$ with a fit to the Curie law in the high (blue line) and low temperature (violet line) regime. The inset shows the magnetic field dependence at 5 K with a linear fit giving χ_{mol} = 4.2×10^{-7} m^3/mol.

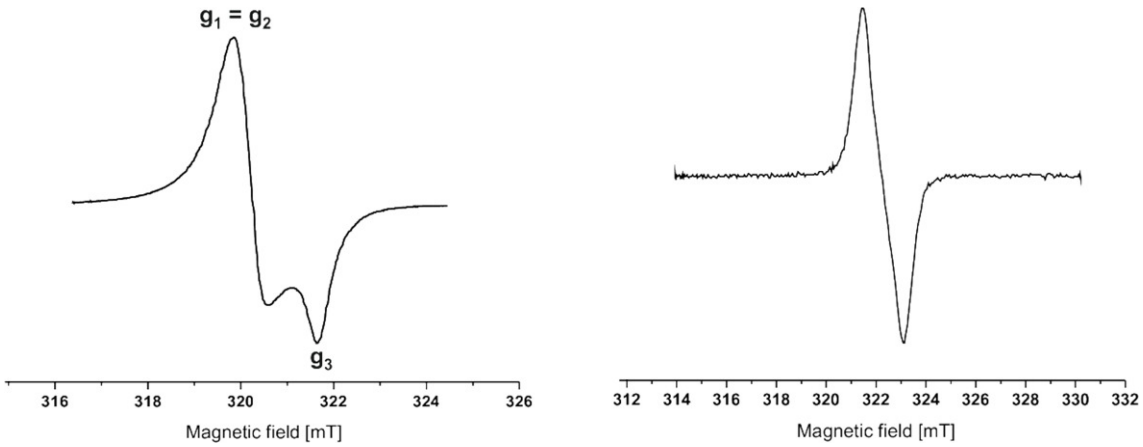

Figure 32. ESR spectrum of **16** in a solid state at 4 K (left) and in a CH_2Cl_2 solution at 294 K (right).

4.3.3 Theoretical studies

Since the oxidation state of the ligands in **15** and **16** cannot be explicitly determined from the X-ray diffraction data, DFT calculations were performed to shed light on the electronic structure and bonding of the ligands. Generally in the non-innocent $C_6H_4(NR)_2$-*o* and $C_6H_4(O)(NR)$-*o* species (R = H, alkyl, aryl), discrimination between the completely reduced amido and phenoxido or oxidized imino and quinone formulation of the ligand is made by inspecting the trends in the experimentally determined C-C, C-N and C-O bond distances, which obviously requires very high quality X-ray diffraction data.[33,74,75] In addition, the partially reduced radical *o*-benzosemiquinone-iminato form should be recognizable by comparison of these bond distances.[76] As earlier studies have shown,[37] computational analyses provide in many cases crucial information for determining the electronic nature of the coordinating ligand and that of the entire complex, especially when the experimental structural data are inconclusive.

In order to determine the correct electronic states of the metals and ligands in both **15** and **16**, the geometries of model complexes **15'** and **16'** (*tert*-butyl substituents replaced with methyl groups) were optimized using the PBE1PBE[77] functional and def2-TZVP[78] basis sets. The nature of the stationary points found was addressed by the subsequent calculation of two of the lowest eigenvalues of the Hessian matrix. Selected geometrical parameters of the optimized structures are given in Table 9.

For **15**, there exist three plausible electronic states: a closed-shell singlet **15'**-S, a high-spin triplet **15'**-T and a broken symmetry singlet diradical **15'**-DR. Geometry optimizations were performed for all of these states and the results indicate that the triplet state is about 30 kJ/mol higher in energy than either of the two singlet states (in agreement with magnetometric measurements), and therefore will not be discussed further. Of the two singlet states, the ground state is the diradical state **15'**-DR, which however is only 5 kJ mol^{-1} lower in energy than **15'**-S. Considering such a small energy difference between these states, the diradical nature of complex **15** is relatively small, which is also evident from the calculated frontier molecular orbitals (MOs; see below). According to the Mulliken population analysis and the calculated spin density,[79] the formally unpaired electrons in **15'**-DR are mostly localized at the nitrogen atoms of the ligand and at the molybdenum center. The diamagnetism in **15'**-DR is then due to the relatively strong antiferromagnetic coupling between these electrons, which results in an S = 0 state.

Table 9. Selected geometrical parameters of **15′** and **16′** as compared with the X-ray data. (For the numbering scheme, see Figures 29 and 30).

		15	**15′**-S	**15′**-DR			**16a**	**16b**	**16**^{AVG}	**16′**-D
Mo	N7	2.065(2)	2.034	2.077	Mo1	N43	2.149(3)	2.152(4)	2.151	2.167
Mo	N7'	2.065(2)	2.042	2.082	Mo1	N50	2.022(3)	2.024(3)	2.023	2.026
Mo	O1	1.982(1)	1.997	1.998	Mo1	O37	2.004(3)	1.997(3)	2.001	1.989
Mo	O1'	1.982(1)	1.966	1.970	Mo1	O52	3.566(4)	3.574(4)	3.570	3.632
O1	C1	1.322(2)	1.312	1.309	O37	C37	1.324(6)	1.344(6)	1.334	1.313
N7	C6	1.398(3)	1.390	1.378	N43	C42	1.375(5)	1.377(6)	1.376	1.357
C1	C2	1.407(3)	1.398	1.400	C37	C38	1.412(6)	1.404(6)	1.408	1.403
C2	C3	1.380(3)	1.384	1.382	C38	C39	1.375(7)	1.385(7)	1.380	1.380
C3	C4	1.411(3)	1.400	1.404	C39	C40	1.415(7)	1.402(6)	1.409	1.407
C4	C5	1.376(3)	1.385	1.382	C40	C41	1.397(6)	1.388(7)	1.393	1.378
C5	C6	1.401(3)	1.396	1.399	C41	C42	1.391(7)	1.401(7)	1.396	1.406
C6	C1	1.400(3)	1.392	1.398	C37	C42	1.426(6)	1.427(5)	1.427	1.421
O1'	C1'	1.322(2)	1.309	1.307	O52	C52	1.375(6)	1.374(5)	1.375	1.345
N7'	C6'	1.398(3)	1.387	1.376	N50	C51	1.431(5)	1.445(6)	1.438	1.424
C1'	C2'	1.407(3)	1.399	1.401	C52	C53	1.403(6)	1.414(7)	1.409	1.401
C2'	C3'	1.380(3)	1.383	1.381	C53	C54	1.395(7)	1.382(6)	1.389	1.384
C3'	C4'	1.411(3)	1.402	1.405	C54	C55	1.400(9)	1.390(8)	1.395	1.394
C4'	C5'	1.376(3)	1.385	1.382	C55	C56	1.378(6)	1.386(7)	1.382	1.385
C5'	C6'	1.401(3)	1.398	1.401	C56	C51	1.397(7)	1.390(6)	1.394	1.393
C6'	C1'	1.400(3)	1.390	1.398	C51	C52	1.390(8)	1.376(8)	1.383	1.397
N7	C8	1.388(2)	1.375	1.369	N43	C44	1.359(5)	1.367(5)	1.363	1.350
N7'	C8'	1.388(2)	1.375	1.369	N50	C49	1.383(5)	1.383(6)	1.383	1.372
C8	C9	1.405(3)	1.396	1.398	C44	C49	1.422(6)	1.442(7)	1.432	1.428
C9	C10	1.378(3)	1.392	1.394	C44	C45	1.412(6)	1.397(6)	1.405	1.407
C10	C10'	1.391(3)	1.396	1.398	C45	C46	1.374(5)	1.372(6)	1.373	1.375
C10'	C9'	1.378(3)	1.381	1.379	C46	C47	1.389(6)	1.397(7)	1.393	1.398
C9'	C8'	1.405(3)	1.381	1.379	C47	C48	1.378(6)	1.374(6)	1.376	1.378
C8'	C8	1.401(3)	1.400	1.407	C48	C49	1.406(5)	1.389(5)	1.398	1.400

A detailed comparison between the X-ray data of **15** and the theoretical results for **15′**-S and **15′**-DR shows a good overall agreement, although some differences can be observed. For both complexes, the largest deviation between the calculated and experimental bond lengths is about 0.04 Å and all important bond lengths in the complex (including those in the *o*-phenylenediamine and *o*-aminophenol rings) are reproduced with good precision (R_{par}[80] values 0.0072 and 0.0045, respectively). The single largest difference between the structures **15′**-S and **15′**-DR is in the Mo-N bond distances which are about 0.04 Å longer in **15′**-DR and thereby in a slightly better agreement with the experimental data. However, the differences in the optimized bond lengths of **15′**-S and **15′**-DR are in general too small in order for any definite conclusions to be drawn about the nature of the electronic ground state of **15**.

The concept of metrical oxidation state (MOS) can be used to quantify the formal oxidation state of non-innocent (oxidized) amidophenoxide or catecholate ligands coordinated to metal ions by examining their geometrical parameters.[35] The MOS calculated for the experimental structure **15** is 1.55(14). The corresponding values for the DFT-optimized structures **15′**-S and **15′**-DR are 1.58(17) and 1.47(15), respectively. From these, the data for **15′**-S are in a slightly better agreement with the experimental value although the estimated standard deviations are very high, preventing definite conclusions. Compounds with metal ions in a high oxidation state and with two or fewer d electrons, such as molybdenum(VI) and vanadium(V) complexes, tend to have non-integer MOS values, which originate from ligand-to-metal π-donation rather than from an antiferromagnetic coupling of electrons residing in separate orbitals.[35] Considering complex **15**, a visual inspection of frontier MOs of **15′**-S and **15′**-DR shows significant delocalization, which in both cases gives rise to π-bonding between the *o*-phenylenediamine fragment of the ligand and the molybdenum ion (Figure 33). This not only explains the similarity of the calculated MOS values for **15′**-S and **15′**-DR, but it also supports the earlier conclusions of the rather small effect that the diradical character has on the overall electronic structure of **15′** (see above).

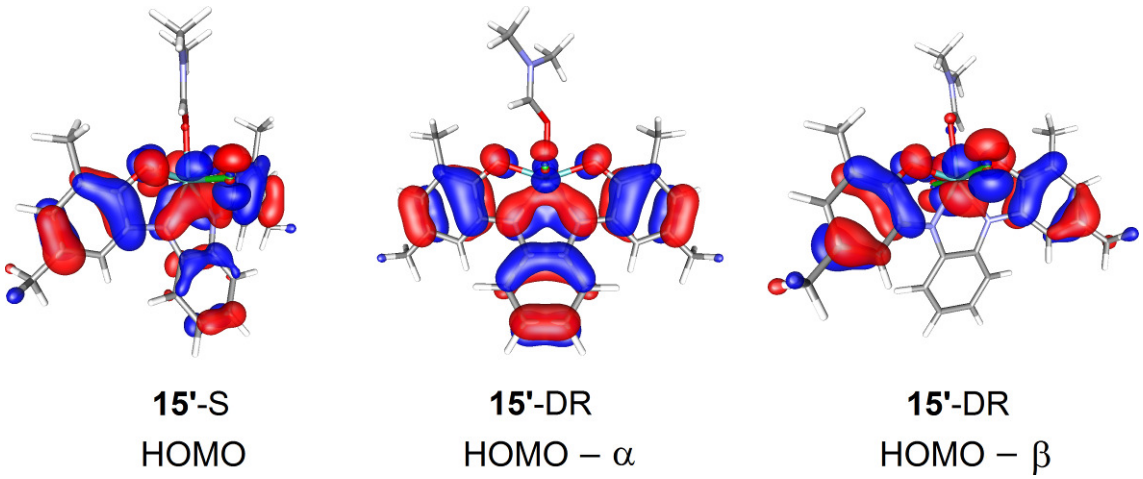

Figure 33. Frontier MOs of **15′**-S and **15′**-DR.

Although the experimental structural data show some discrepancies between the expected and observed bond lengths, the results from theoretical calculations indicate that the ground state of **15** is a singlet with a small diradical character, and which therefore cannot be fully described with a closed-shell configuration. The observed deviations in the geometrical parameters of the phenyl rings and Mo-N/O bonds can be primarily attributed to π-donation from the ligand to the high-valent molybdenum cation, rather than actual electron transfer creating a lower-oxidation-state Mo(V) center.

In a fashion similar to **15**, the geometrical parameters of the tridentate ligand in complex **16** suggest some variation in the oxidation state of the ligand, which is also evident from the odd number of electrons in this complex. The

plausible electronic states for **16** are a doublet (**16'**-D) and a quartet (**16'**-Q). Thus, DFT optimizations were performed to estimate the energy difference between the two states and the results show the quartet state to be over 80 kJ/mol higher in energy compared to the doublet. It is important to note that a broken symmetry doublet with two unpaired electrons at the ligand and one at the metal center (coupled antiferromagnetically as in **15'**-DR) is also a plausible electronic configuration. However, we were not able to locate a minimum corresponding to such a state; the Mulliken populations in the HOMO (SOMO-1) orbital of **16'**-D have also insignificant (only a few percent) contributions from the metal orbitals, thus excluding the possibility of a broken-symmetry type state. Hence, the ground state of complex **16** was inferred to be a pure doublet, which is fully supported by the data from magnetometric measurements (see above).

The theoretical model **16'**-D reproduces the experimental geometrical features of **16** with good to excellent precision (the R_{par} value for bond distances from Table 9 is 0.0056, excluding the distance between the uncoordinated O52 and Mo1). The calculated data reproduce the key bond lengths around the metal center and show that the Mo-N(radical) bond length is significantly longer (by over 0.1 Å) compared to the Mo-N(amido) bond. The structural parameters also show the overall shortening of bonds around the N43 center compared to the amido nitrogen, as the latter bonds are about 0.02 to 0.07 Å longer than the former. In addition, small changes in the C-C and C-O bond distances of the neighboring phenyl groups of N43 indicate delocalization of the unpaired electron density over the whole aromatic system. The delocalization is also visible in the calculated spin distribution of **16'** (Figure 34) which, together with the Mulliken population analysis, shows the unpaired electron to be delocalized over the aromatic rings of the tridentate ligand with roughly one third of the total spin density attributable to the N43 atom.

MOSs were calculated for the experimental structure of **16** (two separate molecules in the asymmetric unit) and for the theoretical model **16'**-D. The MOS calculated for **16** from the average experimental bond distances is 1.50(7), whereas the MOSs calculated separately for the individual molecules in the asymmetric unit are 1.42(10) and 1.58(6). The corresponding MOS value for the DFT-optimized structure is 1.30(9), which differs slightly from the experimental data although the differences are again within 2σ. These results clearly point out the sensitivity of the MOS analysis to the quality of the X-ray data, which prevents an in-depth discussion of the electronic structure of **16**. Similarly to **15**, the calculated non-integer MOSs can be attributed to π-donation from the ligand to the high-valent molybdenum cation (with the formal oxidation state Mo(VI)), rather than to any actual ligand-to-metal electron transfer.

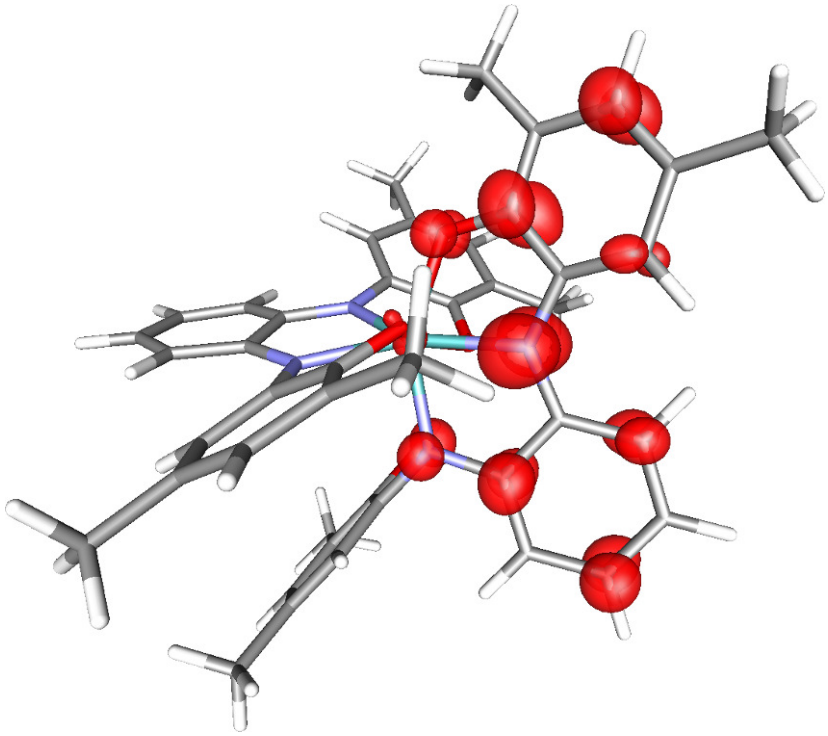

Figure 34. Calculated spin density distribution of complex **16**.

Considered as a whole, the conducted experimental and theoretical investigations present an unambiguous picture of the electronic state and bonding in **16**. To the best of our knowledge, this complex represents the first example of a stable high-valent molybdenum-amidophenoxide radical.

In summary, the potentially tetradentate ligand H_4**L6** has been shown to behave as redox non-innocent in complexation reactions with different molybdenum sources; $[MoO_2(acac)_2]$ and $[MoO_2Cl_2(dmf)_2]$. These reactions produce unexpected and even unprecedented heptacoordinated molybdenum complexes **15** and **16**. The prepared complexes are also rare examples of molybdenum (VI) ions without any multiply-bonded terminal ligands. Hence, the removal of both Mo=O fragments might be facilitated by the redox activity of the ligand.

5 CONCLUSIONS

Four different types of amino- and amidophenolate ligands and their transition metal complexes were studied in this dissertation. The prepared group of 16 complexes presents a fascinating cross-section of the coordination chemistry of this class of ligands. The studied compounds differ from each other mainly by the hapticity and nature of the amine group while still retaining the basic coordinating framework of phenolate oxygen and amino/amido nitrogen. The dissertation illustrates how diverse complexes with novel behavior and properties can be acquired with relatively subtle changes in the ligand backbone.

Synthesis, structure, reactivity and magnetic properties of 12 new first-row transition metal complexes were described in the first part of this study. Three of these were dinuclear iron(III) complexes with tridentate aminophenol ligands while the rest 9 form a family of di- and trinuclear mixed-valence Mn(II)/Mn(III) complexes bearing ligands with up to seven donor atoms. The complexes inside the groups are closely related and by inspecting the geometrical parameters determined by X-ray crystallography, certain correlations between their structure and magnetic behavior can be stated. Furthermore, the detailed DFT studies performed describe the exchange coupling in the complexes with good accuracy and completely support the proposed correlations between the structure and magnetic behavior of these compounds.

In the second part of the dissertation, four novel 4d and 5d transition metal complexes with amino- and amidophenolate ligands were prepared and characterized with an extensive selection of methods. The solid- and solution-state structures of imidotungsten(VI) complexes with bidentate structurally non-innocent aminophenol ligands were determined with X-ray crystallographic and NMR methods. Furthermore, the unexpected reactivity of the ligands and complexes was elucidated both theoretically and experimentally. In addition, two examples of rare Mo(VI) complexes without any multiply-bonded ligands were prepared using potentially tetradentate, electronically non-innocent amidophenolate ligand and thoroughly characterized by experimental and theoretical methods.

The research performed for this dissertation demonstrates the versatility of polydentate aminophenol ligands in two distinct manners. First, these compounds can be utilized to synthesize a series of 3d transition metal complexes which in turn could be further used to predict and interpret the magnetic properties of a certain group of compounds. Second, the unrecognized reactivity and electronic non-innocent behavior of these ligands can be exploited to produce novel metal complexes exhibiting exceptional chemical and physical properties.

REFERENCES

1 Atkins, P. W.; Overton, T.L.; Rourke, J.P.; Weller, M.T.; Armstrong, F.A. *Shriver and Atkins' Inorganic Chemistry*, 5th edition, Oxford University Press, New York, **2010**.

2 Gatteschi, D.; Sessoli, R.; Villain, J. *Molecular Nanomagnets*, Oxford University Press, New York, **2006**.

3 Wichmann, O.; Sillanpää, R.; Lehtonen, A. *Coord. Chem. Rev.* **2012**, *256*, 371.

4 Ambrosi, G.; Formica, M.; Fusi, V.; Giorgi, L.; Micheloni, M. *Coord. Chem. Rev.* **2008**, *252*, 1121.

5 (a) Blackmore, K. J.; Lal, N.; Ziller, J. W.; Heyduk, A. F. *J. Am. Chem. Soc.* **2008**, *130*, 2728. (b) Blackmore, K. J.; Lal, N.; Ziller, J. W.; Heyduk, A. F. *Eur. J. Inorg. Chem*. **2009**, 735. (c) Chauduri, P.; Hess, M.; Müller, J.; Hildenbrand, K. ; Bill, E.; Weyhermüller, T.; Wieghardt, K. *J. Am. Chem. Soc.* **1999**, *121*, 9599.

6 Wichmann, O.; Sopo, H.; Lehtonen, A.; Sillanpää, R. *Eur. J. Inorg. Chem.* **2011**, 1283.

7 Kahn, O. *Molecular Magnetism*, VCH Weinheim, **1993**.

8 Karotsis, G.; Evangelisti, M.; Dalgarno, S. J.; Brechin, E. K. *Angew. Chem. Int. Ed.* **2009**, *48*, 9928.

9 (a) Gatteschi, D.; Sessoli, R. *Angew. Chem. Int. Ed.* **2003**, *42*, 268. (b) Dei, A.; Gatteschi, D. *Angew. Chem. Int. Ed.* **2011**, *50*, 11852. (c) Katoh, K.; Isshiki, H.; Komeda, T.; Yamashita, M. *Chem.–Asian. J.* **2012**, *7*, 1154.

10 (a) Mannini, M.; Pineider, F.; Danieli, C.; Totti, F.; Sorace, L.; Sainctavit, P.; Arrio, M. A.; Otero, E.; Joly, L.; Cezar, J. C.; Cornia, A.; Sessoli, R. *Nature* **2010**, *468*, 417. (b) Urdampilleta, M.; Nguyen, N. V.; Cleuziou, J. P.; Klyatskaya, S.; Ruben, M.; Wernsdorfer, W. *Int. J. Mol. Sci.* **2011**, *12*, 6656. (c) Leuenberger, M. N.; Loss, D. *Nature* **2001**, *410*, 789. (d) Ardavan, A.; Rival, O.; Morton, J. J. L.; Blundell, S. J.; Tyryshkin, A. M.; Timco, G. A.; Winpenny, R. E. P. *Phys. Rev. Lett.* **2007**, *98*, 057201.

11 (a) Sessoli, R.; Gatteschi, D.; Caneschi, A.; Novak, M.A. *Nature* **1993**, *365*, 141. (b) Christou, G.; Gatteschi, D.; Hendrickson, D.N.; Sessoli, R. *Mater. Res. Bull.* **2000**, *25*, 66. (c) Aubin, S.M.J.; Wemple, M.W.; Adams, D.M.; Tsai, H.-L. ; Christou, G.; Hendrickson, D.N. *J. Am. Chem. Soc.* **1996**, *118* ,7746.

12 Lis, T. *Acta Crystallogr.* **1980**, *B36*, 2042.

13 Sessoli, R.; Tsai, H.L.; Schake, A.R.; Wang, S.Y.; Vincent, J.B.; Folting, K.; Gatteschi, D.; Christou, G.; Hendrickson, D.N. *J. Am. Chem. Soc.* **1993**, *115*, 1804.

14 Caneschi, A.; Gatteschi, D.; Sessoli, R.; Barra, A. L.; Brunel, L. C.; Guillot, M. *J. Am. Chem. Soc.* **1991**, *113*, 5873.

15 Milios, C. J.; Vinslava, A.; Wernsdorfer, W.; Moggach, S.; Parsons, S.; Perlepes, S. P.; Christou, G.; Brechin, E. K. *J. Am. Chem. Soc.* **2007**, *129*, 2754.

16 Thomas, L.; Lionti, F.; Ballou, R.; Gatteschu, D.; Sessoli, R.; Barbara, B. *Nature* **1996** ,*383*, 145.

17 Ako, A. M.; Hewitt, I. J.; Mereacre, V.; Clérac, R.; Wensdorfer, W.; Anson, C. E.; Powell, A. K. *Angew. Chem., Int. Ed.* **2006**, *45*, 4926.

18 Winpenny, R. E. P. *J. Chem. Soc. Dalton Trans. 1*, **2002**, 1.

19 (a) T. Glaser, *Chem. Commun.*, **2011**, *47*, 116. (b) Glaser, T.; Theil, H.; Heidemeier, M. *C. R. Chimie*, **2008**, *11*, 1121.

20 Roubeau, O.; Clérac, R. *Eur. J. Inorg. Chem.* **2008**, 4325.

21 Getzlaff, M. *Fundamentals of Magnetism*, Springer Berlin Heidelberg New York, **2008**.

22 (a) J. B. Goodenough, *Phys. Rev.* **1955**, *100*, 564.; (b) Anderson, P. W. *Phys. Rev.* **1959**, *115*, 2. (c) J. Kanamori, J. *Phys. Chem. Solids* **1959**, *10*, 87.

23 Hatfield, W. E. *Inorg. Chem.* **1983**, *22*, 833.

24 Robin, M.B.; Day, P. *Adv. Inorg. Chem. Radiochem.* **1967**, *10*, 247.

25 Rinehart, J. D.; Long, J. R. *Chem. Sci.* **2011**, *2*, 2078.

26 Tuna, F.; Smith, C. A.; Bodensteiner, M.; Ungur, L.; Chibotaru, L. F.; McInnes, E. J. L.; Winpenny, R. E. P.; Collison, D.; Layfield, R. A. *Angew. Chem., Int. Ed.* **2012**, *51*, 6976.

27 Rinehart, J. D.; Fang, M.; Evans, W. J.; Long, J. R. *J. Am. Chem. Soc.* **2011**, *133*, 14236.

28 Oshio, H.; Nakano, M. *Chem. Eur. J.* **2005**, *11*, 5178.

29 Goswami, T.; Anirban, M. *J. Phys. Chem. A.* **2012**, *116*, 5207.

30 Jurca, T.; Farghal, A.; Lin, P.-H.; Korobkov, I.; Murugesu, M.; Richeson, D. S. *J. Am. Chem. Soc.* **2011**, *133*, 15814.

31 (a) Sylvester, K. T.; Chirik, P. J. *J. Am. Chem. Soc.* **2009**, *130*, 8772. (b) Smith, A. L.; Hardcastle, K. I.; Soper, J. D. *J. Am. Chem. Soc.* **2010**, *132*, 14358. (c) Wieder, N. L.; Gallagher, M.; Carroll, P. J.; Berry, D. H. *J. Am. Chem. Soc.* **2010**, *132*, 4107.

32 Jørgensen, C. K. *Coord. Chem. Rev.* **1966**, *1*, 164.

33 (a) Kaim, W.; Schwederski, B. *Coord. Chem. Rev.* **2010**, *254*, 1580. (b) Kaim, W. *Inorg. Chem.* **2011**, *50*, 9752. (c)

34 Chun, H.; Chaudhuri, P.; Weyhermüller, T.; Wieghardt, K. *Inorg. Chem.* **2002**, *41*, 790. (b) Pierpont, C. G.; Buchanan, R. M. *Coord. Chem. Rev.* **1981**, *38*, 45.

35 Brown, S. N. *Inorg. Chem.* **2012**, *51*, 1251.

36 (a) Blanchard, S.; Derat, E.; Desage-El Murr, M.; Fensterbank, L.; Malacria, M.; Mouriès-Mansuy, V. *Eur. J. Inorg. Chem.* **2012**, 376. (b) Dunn, T. J.; Ramogida, C. F.; Simmonds, C.; Paterson, A.; Wong, E. W. Y.; Chiang, L.; Shimazaki, Y.; Storr, T. *Inorg. Chem.* **2011**, *50*, 6746.

37 (a) Bachler, V.; Olbrich, G.; Neese, F.; Wieghardt K. *Inorg. Chem.* **2002**, *41*, 4179. (b) Das, D.; Sarkar, B.; Mondal, T. K.; Mobin, S. M.; Fiedler, J.; Kaim, W.; Lahiri, G. M. *Inorg. Chem.* **2011**, *50*, 7090. (c) Lu, C. C.; DeBeer George, S.; Weyhermüller, T.; Bill, E.; Bothe, E.; Wieghardt, K. *Angew. Chem., Int. Ed.* **2008**, *47*, 6384. (d) Tomson, N. C.; Labios, L. A.; Weyhermüller, T.; Figueroa, J. S.; Wieghardt, K. *Inorg. Chem.* **2011**, *50*, 5763.

38 Potember, R. S.; Poehler, T. O.; Cowan, D. O. *Appl. Phys. Lett.* **1979**, *34*, 405.

39 (a) Zhao, H.; Bazile Jr., M. J.; Galán-Mascarós, J. R.; Dunbar, K. R. *Angew. Chem. Int. Ed.* **2003**, *42*, 1015 (b) Harris, T. D.; Coulon, C.; Clérac, R.; Long, J. R. *J. Am. Chem. Soc.* **2011**, *133*, 123.

40 Chirik, P. J.; Wieghardt, K. *Science* **2010**, *327*, 794.

41 McCleverty, J. A.; Meyer, T. J. *Comprehensive Coordination Chemistry II*, Elsevier, **2003**.

42 (a) Cha, M.; Shoner, S. C.; Kovacs, J. A. *Inorg. Chem.* **1993**, **32**, 1860. (b) Melson, G. A.; Busch, D. H. *J. Am. Chem. Soc.* **1964**, *86*, 4834. (c) Bokach, N. A.; Kukushkin, V. Yu.; Kuznetsov, M. L.; Garnovskii, D. A.; Natile, G.; Pombeiro, A. J. L. *Inorg. Chem.* **2002**, *41*, 2041.

43 Lesh, F.D.; Lord, R. L.; Heeg, M. J.; Schlegel, H. B.; Verani, C. N. *Eur. J. Inorg. Chem.* **2012**, 463.

44 van der Vlugt, J. I. *Eur. J. Inorg. Chem.* **2012**, 363

45 Egdal, R. K.; Larsen, F. B.; Bond, A. D.; McKenzie, C. J. *Inorg. Chim. Acta* **2005**, *358*, 376.

46 Day, G.S.; Pan, B.; Kellenberger, D. L.; Foxman, B. M.; Thomas, C. M. *Chem. Comm.* **2011**, *47*, 3634.

47 Sgro, M. J.; Stephan, D. W. *Dalton Trans.* **2011**, *40*, 2419.

48 Dugan, T. R.; Bill, E.; MacLeod, K. C.; Christian, G. J.; Cowley, R. E.; Brennessel, W. W.; Ye, S.; Neese, F.; Holland, P. L. *J. Am. Chem. Soc.* **2012**, *134*, 20352.

49 Riisiö, A.; Wichmann, O.; Sillanpää, R. *Lett. Org. Chem.* **2010**, *7*, 298.

50 (a) Crabtree, R. H.; Hlatky, G. G. *Polyhedron*, **1985**, *4*, 521. (b) Bradley, D. C.; Hursthouse, M. B.; Abdul Malik, K. M.; Nielson, A. J.; Short, R. L. *J. Chem. Soc., Dalton Trans.*, **1983**, 2651.

51 CrysAlisPro, **2013**, Agilent Technologies Ltd, Yarnton, England.

52 Sheldrick, G. M. SADABS., University of Göttingen, Germany, **2008**.

53 Sheldrick, G. M. *Acta Crystallogr., Sect. A: Found. Crystallogr.* **2008**, 64, 112.

54 Altomare, A.; Burla, M. C.; Camalli, M.; Cascarano, G. L.; Giacovazzo, C.; Guagliardi, A.; Moliterni, A. G. G.; Polidori, G.; Spagna, R. *J. Appl. Crystallogr.* **1999**, *32*, 115.

55 (a) *Diamond - Crystal and Molecular Structure Visualization*, Crystal Impact - Dr. H. Putz & Dr. K. Brandenburg GbR, Kreuzherrenstr. 102, 53227 Bonn, Germany. (b) *Mercury CSD 2.0* - New Features for the Visualization and Investigation of Crystal Structures, Macrae, C. F.; Bruno, I. J.; Chisholm, J. A.; Edgington, P. R.; McCabe, P.; Pidcock, E.; Rodriguez-Monge, L.; Taylor, R.; van de Streek, J.; Wood, P. A. *J. Appl. Cryst.* **2008**, *41*, 466.

56 (a) *Gaussian 03,* Revision C.02, Frisch, M. J.; Trucks, G. W.; Schlegel, H. B.; Scuseria, G. E.; Robb, M. A.; Cheeseman, J. R.; Montgomery, Jr., J. A.; Vreven, T.; Kudin, K. N.; Burant, J. C.; Millam, J. M.; Iyengar, S. S.; Tomasi, J.; Barone, V.; Mennucci, B.; Cossi, M.; Scalmani, G.; Rega, N.; Petersson, G. A.; Nakatsuji, H.; Hada, M.; Ehara, M.; Toyota, K.; Fukuda, R.; Hasegawa, J.; Ishida, M.; Nakajima, T.; Honda, Y.; Kitao, O.; Nakai, H.; Klene, M.; Li, X.; Knox, J. E.; Hratchian, H. P.; Cross, J. B.; Bakken, V.; Adamo, C.; Jaramillo, J.; Gomperts, R.; Stratmann, R. E.; Yazyev, O.; Austin, A. J.; Cammi, R.; Pomelli, C.; Ochterski, J. W.; Ayala, P. Y.; Morokuma, K.; Voth, G. A.; Salvador, P.; Dannenberg, J. J.; Zakrzewski, V. G.; Dapprich, S.; Daniels, A. D.; Strain, M. C.; Farkas, O.; Malick, D. K.; Rabuck, A. D.; Raghavachari, K.; Foresman, J. B.; Ortiz, J. V.; Cui, Q.; Baboul, A. G.; Clifford, S.; Cioslowski, J.; Stefanov, B. B.; Liu, G.; Liashenko, A.; Piskorz, P.; Komaromi, I.; Martin, R. L.; Fox, D. J.; Keith, T.; Al-Laham, M. A.; Peng, C. Y.; Nanayakkara, A.; Challacombe, M.; Gill, P. M. W.; Johnson, B.; Chen, W.; Wong, M. W.; Gonzalez, C.; and Pople, J. A.; Gaussian, Inc., Wallingford CT, 2004. (b) *TURBOMOLE V6.3 2011*, a development of University of Karlsruhe and Forschungszentrum Karlsruhe GmbH, 1989−2007, TURBOMOLE GmbH since 2007; available from http://www.turbomole.com.

57 (a) Thompson, L. K.; Mandal, S. K.; Tandon, S. S.; Bridson, J. N.; Park, M. K. *Inorg. Chem.* **1996**, *35*, 3117. (b) Wichmann, O.; Sopo, H.; Colacio, E.; Mota, A.; Sillanpää, R. *Eur. J. Inorg. Chem.* **2009**, 4877; (c) Venegas-Yazigia, D.; Aravena, D.; Spodine, E.; Ruiz, E.; Alvarez, S. *Coord. Chem. Rev.* **2010**, *254*, 2086. (d) Seppälä, P.; Colacio, C.; Mota, A. J.; Sillanpää, R. *Dalton Trans.* **2012**, *41*, 2648. (e) Riisiö, A.; Hänninen, M. M.; Sillanpää, R. *Eur. J. Inorg. Chem.* **2012**, 1048.

58 (a) Ball, J. I.; Morgan, C. H. *Acta Cryst*. **1967**, *23*, 239; b) Yoshida, J. Nishikiori, S.; Kuroda, R. *Chem.- Eur. J.* **2008**, *14*, 10570

59 (a) van Gorkum, R.; Berding, J.; Mills, A. M.; Kooijman, H.; Tooke, D. M.; Spek, A. L.; Mutikainen, I.; Turpeinen, U.; Reedijk, J.; Bouwman E. *Eur. J. Inorg. Chem.* **2008**, *2008*, 1487. (b) Neves, A.; Rossi, L. M.; Vencato, I.; Haase, W.; Werner, R. *J. Chem. Soc., Dalton Trans*. **2000**, 707. (c) Neves, A.; de Brito, M. A.; Vencato, I.; Drago, V.; Griesar, K.; Haase W. *Inorg. Chem.* **1996**, *35*, 2360.

60 Addison, A. W.; Rao, T. N.; Reedijk, J.; van Rijn, J.; Verschcoor, G. C. *J. Chem. Soc., Dalton Trans*. **1984**, 1349.

61 (a) Hirotsu, M; Kojima, M.; Mori, W.; Yoshikawa, *Bull. Chem. Soc. Jpn*. **1998**, *71*, 2873. (b) Hirotsu, M; Kojima, M.; Yoshikawa, Y; *Bull. Chem. Soc. Jpn.***1997**, *70*, 649. (c) Schmitt, H.; Lomoth, R.; Magnuson, A.; Park, J.; Fryxelius, J.; Kritikos, M.; Mårtensson, J.; Hammarström, L.; Sun, L.; Åkermark, B. *Chem. Eur. J*. **2002**, *8*, 3757. (d) Anderlund, M.F.; Zheng, J.; Ghiladi, M.; Kritikos, M.; Riviere, E.; Sun, L.; Girerd, J.-J.; Akermark, B. *Inorg. Chem. Commun*. **2006**, *9*, 1195.

62 Werner, R.; Ostrovsky, S.; Griesar, K.; Haase, W. *Inorg. Chim. Acta*, **2001**, *326*, 78.

63 (a) Zener, C. *Phys. Rev*. **1951** *82*, 403–405 (b) Girerd, J.-J. *J. Chem. Phys.* **1983** *79*, 1766.

64 Lehtonen, A.; Balcar, H.; Sedláĉek, J.; Sillanpää, R. *J. Organomet. Chem.* **2008**, *693*, 1171.

65 Coe, B. J.; Glenwright, S. J. *Coord. Chem. Rev*. **2000**, *203*, 5.

66 van der Schaaf, P. A.; Boersma, J.; Smeets, W. J. J.; Spek, A. L.; van Koten, G. *Inorg. Chem*. **1993**, *32*, 5108.

67 (a) Motevalli, M.; Parkin, B. C.; Ramnauth, R.; Sullivan, A. C. *J. Chem. Soc., Dalton Trans.* **2000**, 2661. (b) Dreisch, K.; Andersson, C.; Stålhandske, C. *Polyhedron* **1993**, *12*, 1335.

68 Yu, S.; Holm, R. H. *Inorg. Chem*. **1989**, *28*, 4385.

69 Gross, K. C.; Seybold, P. G.; Hadad, C. M. *Int. J. Quantum Chem.* **2001**, *90*, 445.

70 Casanova, D.; Alemany, P.; Bofill, J. M.; Alvarez, S. *Chem. Eur. J.* **2003**, *9*, 1281.

71 Mohn, P. *Magnetism in the solid state - an introduction*, Springer-Verlag, Berlin, **2003**.

72 (a) Ottenwaelder, X; Ruiz-García, R.; Blondin, G.; Carasco, R.; Cano, J.; Lexa, D.; Journaux Y.; Aukauloo, A. *Chem. Commun.* **2004**, 504. (b)

Waldhör, E.; Schwederski, B.; Kaim, W. *J. Chem. Soc., Perkin Trans. 2* **1993**, 2109.

73 Xiao, Z.; Bruck, M. A.; Doyle, C.; Enemark, J. H.; Grittini, C.; Gable, R. W.; Wedd, A. G.; Young, C. G. *Inorg. Chem.* **1995**, *34*, 5950.

74 Khusniyarov, M. M.; Harms, K.; Burghaus, O.; Sundermeyer, J.; Sarkar, B.; Kaim, W.; van Slageren, J.; Duboc, C.; Fiedler, J. *Dalton Trans*. **2008**, 1355.

75 Chaudhuri, P.; Verani, C. N.; Bill, E.; Bothe, E.; Weyhermüller, T.; Wieghardt, K. *J. Am. Chem. Soc.* **2001**, *123*, 2213.

76 Bhattacharya, S.; Gupta, P.; Basuli, F.; Pierpont, C. G. *Inorg. Chem.* **2002**, *41*, 5810.

77 (a) Perdew, J. P.; Burke, K.; Ernzerhof, M. *Phys. Rev. Lett.* **1996**, *77*, 3865. (b) Perdew, J. P.; Burke, K.; Ernzerhof, M. *Phys. Rev. Lett.* **1997**, *78*, 1396. (c) Perdew, J. P.; Ernzerhof, M.; Burke, K. *J. Chem. Phys.* **1996**, *105*, 9982. (d) Adamo, C.; Barone, V. *J. Chem. Phys.* **1999**, *110*, 6158.

78 (a) Weigend, F.; Häser, M.; Patzelt, H.; Ahlrichs, R. *Chem. Phys. Lett.* **1998**, *294*, 143. (b) Weigend, F.; Ahlrichs, R. *Phys. Chem. Chem. Phys.* **2005**, *7*, 3297.

79 Mulliken, R. S., *J. Chem. Phys.* **1955**, *23*, 1833.

80 R_{par} is defined as $R_{par} = \frac{\Sigma(|P_{exp} - P_{theo}|)}{\Sigma(|P_{exp}|)}$ and can be used to quantitatively measure the fit of theoretical model to experimental one.